Renewable and Sustainable Energy Reviews 217 (2025) 115709

Contents lists available at ScienceDirect

Renewable and Sustainable Energy Reviews

journal homepage: www.elsevier.com/locate/rser

Impacts of photovoltaics and integrated green roofs on urban climate: Experimental insights for urban land surface modelling

Liutao Chen [a,b], Zinan Lin [a], Qi Zhou [a], Shihong Zhang [a], Mengying Li [c], Zhe Wang [a,b,*]

[a] Department of Civil and Environmental Engineering, The Hong Kong University of Science and Technology, Hong Kong Special Administrative Region of China
[b] HKUST Shenzhen-Hong Kong Collaborative Innovation Research Institute, Futian, Shenzhen, China
[c] Department of Mechanical Engineering & Research Institute for Smart Energy, The Hong Kong Polytechnic University, Hong Kong Special Administrative Region of China

ARTICLE INFO

Keywords:
Photovoltaic (PV) panels
Photovoltaic integrated green roofs (PVIGR)
Building envelope
Urban heat island (UHI)
Urban energy balance
Building energy consumption

ABSTRACT

Previous studies examining the impact of large-scale photovoltaic (PV) roofs on urban heat islands (UHI) have reported inconsistencies, primarily due to reliance on simulations without robust experimental validation. This study addresses this gap through a six-month experimental investigation of four 200 m^2 rooftop sites in subtropical Hong Kong. We compared a conventional bare roof, a PV roof, and two PV integrated green roofs (PVIGRs), providing the first real-world comparison of these configurations.

Results reveal that hourly air temperatures above PV rooftops exceeded those above bare roof by over 4 °C on sunny days, with a monthly peak PV heat island (PVHI) intensity of 1.18 °C at noon in July. The PVHI was primarily driven by PV surface temperatures, solar irradiance, and ambient air temperatures. Additionally, a notable PV-canopy heating effect was observed under PV panels. While PVIGRs did not exhibit cooling above panels, they mitigated the heating effect underneath by up to 1.26 °C in July, lowering PV surface temperatures and building heat conduction. This dual benefit enhances PV efficiency and reduces buildings cooling loads.

These findings suggest refining urban land surface models to better estimate the climatic consequences of widespread PV installations. The proposed PV parameterization scheme should consider the heating effects beneath PV canopies and surface roughness length of PV configurations. Additionally, integrated building energy models with urban canopy models could help simulate waste heat from air conditioning influenced by PV rooftops. These insights can inform urban planning and efficient PV deployment strategies.

1. Introduction

1.1. Background

Urban Heat Island (UHI) is a phenomenon where urban areas are warmer than their rural surroundings [1]. This temperature disparity leads to various adverse effects, including increased heat-related mortality risks [2,3], higher energy demand for cooling [4,5], and exacerbated urban heat due to waste heat emissions [6,7]. These issues create a vicious cycle that poses significant environmental challenges in the face of global urbanization. Traditional interventions such as cool roofs and green roofs (GR) have been both empirically and theoretically proven to mitigate UHI effects and enhance building energy efficiency, particularly in hot climates [8,9].

In recent years, the global push for renewable energy has highlighted the importance of photovoltaic (PV) roofs, which generate on-site electricity and reduce building energy consumption [10–12]. However, PV installations also contribute to localized heating, known as the Photovoltaic Heat Island (PVHI) effect [13]. This occurs because PV panels absorb significant solar radiation but convert only a portion into electricity [14], releasing the remainder as heat into the surrounding environment. The heat release elevates local temperatures, creating a feedback loop: as PV surface temperatures rise, their electrical efficiency declines [15], further amplifying excess heat output and exacerbating the PVHI effect.

To mitigate this effect, integrating PV systems with green roofs has emerged as a promising solution [16]. PV-integrated green roofs (PVIGRs) combine energy generation with vegetation, optimizing

* Corresponding author. Department of Civil and Environmental Engineering, The Hong Kong University of Science and Technology, Hong Kong Special Administrative Region of China.
E-mail address: cezhewang@ust.hk (Z. Wang).

https://doi.org/10.1016/j.rser.2025.115709
Received 20 September 2024; Received in revised form 3 April 2025; Accepted 3 April 2025
Available online 12 April 2025
1364-0321/© 2025 Elsevier Ltd. All rights reserved, including those for text and data mining, AI training, and similar technologies.

rooftop space for multifunctionality [17,18]. The cooling effects of greenery beneath PV panels can lower surface temperatures, enhancing PV cell's efficiency, improving building insulation, and reducing cooling energy needs [19–23]. This synergy not only boosts power generation efficiency—the primary and initial aim—but also has the potential to mitigate UHI effects and increase biodiversity [16,19,24], thereby contributing to more sustainable urban environments.

Despite these advancements, the broader impact of PV roofs on UHI at neighbourhood and regional scales remains underexplored [14,25]. This knowledge gap persists because most existing studies rely on numerical simulations rather than experimental data. Since alterations to the surface energy balance directly affect air temperatures in urban environments, building energy models like EnergyPlus can effectively quantify convective heat flux from various roof types (bare, green, and white roofs with PV panels) [22,26,27], consistently showing increased convective heat flux with PV installations. However, these tools fundamentally lack the atmospheric physics required to simulate air temperature responses - a critical limitation for UHI research.

To bridge this modelling gap, researchers have developed various PV parameterization schemes in urban land surface models coupled with atmospheric models. These range from simplified effective albedo methods (e.g., in the urbanized MM5 model [28], WRF/SLUCM [29], and CCSM4 [30]) to more complex physically-based schemes (e.g., in the Town Energy Balance model [31], and WRF/BEP + BEM [32,33]). For example, Taha's simulation [28] estimated a 0.2 °C temperature reduction in Los Angeles using high-efficiency PV systems (conversion efficiency $\eta = 30$ %), while more pronounced cooling (0.7 °C peak reduction) was predicted for Phoenix during extreme heat events in July 2009 using rooftop PV panels ($\eta = 14$ %) [32]. At the global scale, Hu et al. [30] found that covering 100 % of urban regions worldwide with PV panels ($\eta = 27$ %) could induce a cooling effect of approximately 0.26 °C. While these studies suggest that PV installations can alleviate UHI effects to some extent, they are often constrained by model assumptions and limited experimental validation, potentially leading to inaccuracies that could misinform policy and decision-making.

The presence of PV systems in cities significantly affect the urban energy balance, as illustrated in Fig. 1. Recent attention has focused on the thermal properties of PV systems, which are characterized by low albedo, low emissivity, and low heat capacity [34]. Such properties lead to decreased upward shortwave and longwave radiation, resulting in higher net radiation absorption during the day (Fig. 1b). At night, the low heat storage capacity facilitates quicker cooling [34]. As a result, PV heats up rapidly after sunrise and releases heat efficiently under sunset. Additionally, PV installations modify the energy balance of building roof by adding a layer that dissipates heat through radiation and convection. This layer also provides shading and reduces the sky view factor for the surface beneath them, thereby diminishing nighttime cooling. In contrast, PVIGR exhibits more complex energy dynamics (Fig. 1c), where vegetation enhances latent heat conversion through evapotranspiration, moderating surface temperatures and altering the overall energy exchanges.

Given the significant impacts of PV systems on urban climate and building energy consumption, a systematic evaluation is essential. Section 1.2 presents a targeted literature review of experimental studies that provide observational evidence of PV impacts on urban climates. We have intentionally excluded simulation-based studies at this stage, because their dependence on inaccurate assumptions may compromise result reliability.

This study adopts a three-phase analytical approach: (1) Section 1.2 synthesizes existing experimental evidence; (2) Section 3 presents field measurements from our experiments; and (3) Section 4.1 critically evaluates existing modelling approaches by comparing their outputs with experimental evidence.

1.2. Literature review

To investigate the impact of photovoltaic (PV) systems on urban climate, a comprehensive literature review was conducted on March 12, 2025, utilizing two primary databases: Web of Science (WOS) and Scopus. Given the focus on experimental studies, the search strategy incorporated the following keywords:

TS = ("PV" OR "Photovoltaic*" OR "solar power" OR "solar cell*" OR "Solar Panel*")

AND TS = ("roof*" OR "green roof")

AND TS = ("measur*" OR "observ*" OR "experiment*" OR "monitor*")

AND TS = ("urban climate" OR "microclimate" OR "urban weather" OR "thermal environment" OR "air temperature*" OR "urban heat island" OR "UHI" OR "urban energy" OR "surface energy")

This search retrieved 150 papers from WOS and 217 papers from Scopus. After deduplication, 244 records remained, with 77 identified as experimental studies. While most experimental studies focus on the inherent advantages of PV systems, such as power generation performance and efficiency, only 10 papers directly address the climate impact

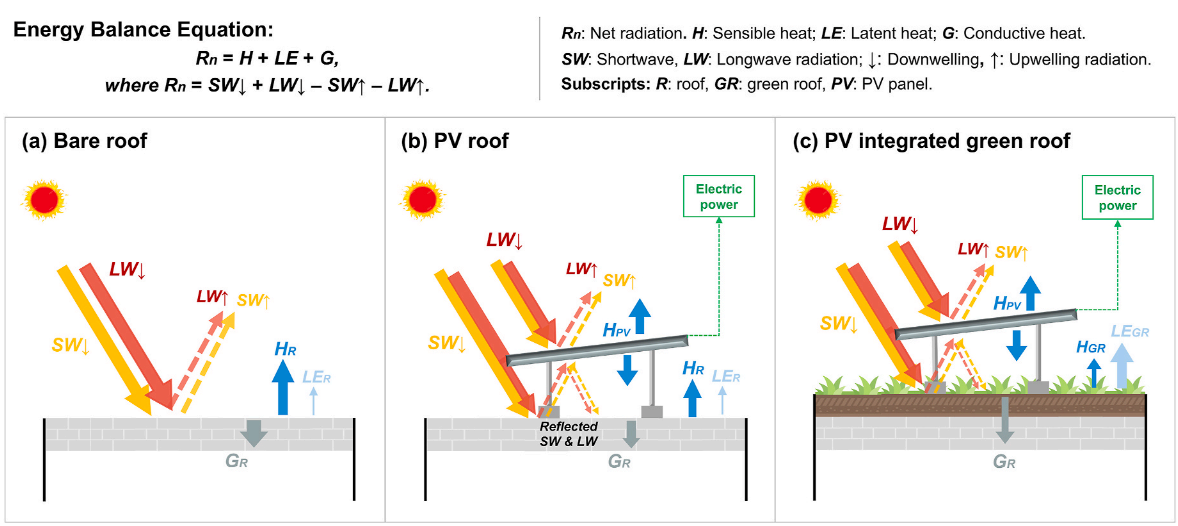

Fig. 1. Energy balance of **(a)** bare roof, **(b)** PV roof, and **(c)** PV integrated green roof. (For interpretation of the references to color in this figure legend, the reader is referred to the Web version of this article.)

of PV deployment, such as effects on near-surface meteorology and surface energy exchanges. This disparity highlights a critical research gap, as experimental efforts have largely prioritized component-level performance over broader climatic implications. Detailed records of the reviewed studies are provided in the Excel file in Supplementary Material.

The 10 studies reviewed span scales ranging from square meters to hectare and can be categorized into three groups.

- **Small-scale**: Individual or few PV panels, scaled-down rooms, and experimental mock-ups.
- **Mid-Scale (over 100 m^2)**: Real building rooftops.
- **Large-Scale (hectare level)**: Utility-scale PV power plants.

Investigating the impact of PV systems on urban climates presents significant challenges. These include the difficulty of identifying comparable urban regions for effective comparative studies, the high labor and equipment costs of setting up and monitoring large-scale experiments, and restricted access to rooftops due to safety regulations and property management. Despite these challenges, the reviewed studies encompass a range of scales, with six small-scale, two mid-scale, and two large-scale experiments specifically addressing the climatic impact of PV. These studies are summarized in Table 1, which highlights study sites, publication years, analysis period, and key findings.

One of the earliest attempts [27] measured PV and rooftop surface temperatures to estimate sensible heat flux, providing valuable insights into each roof type's contribution to the UHI effect. This research highlighted the importance of considering sensible heat flux from both sides of the PV panels and the shaded portion of the roof. This approach was applied in various settings by the same research group led by David Sailor, including ground-mounted PV [35] and scaled-down test building rooftop [26] in Arizona, USA. These studies provided critical estimates of sensible heat from PV systems. However, their reliance on assumption of uniform air temperature distributions above and below panels introduced uncertainty. Additionally, these experiments were limited to the summer conditions, leaving their applicability to other seasons undetermined.

Subsequent studies focused on the climate impacts of large-scale deployment of PV plants, particularly their influence on near-surface air temperature and energy balance [36]. By analysing measured radiative fluxes, researchers observed that PV plants do exert a surface radiative impact and act as energy sinks, particularly during summer months [37]. PV plants increased daytime net radiation by 8.2 % during summer—due to reductions in upward shortwave and longwave radiation, with a slight positive anomaly in winter [37]. Further research highlighted that PV alters surface energy balance by reducing upward longwave emissions and heat storage [34], favouring more efficient sensible heat flux due to their low emissivity, low heat capacity, and increased surface area and roughness. Additionally, PV shading significantly reduces ground heat storage during daytime and nocturnal heat release, underscoring the complex interactions between PV installations and climate dynamics.

However, these large-scale studies were conducted in utility-scale solar power plants, which were situated in environments with land-surface properties vastly different from urban rooftops—leading to distinct atmospheric boundary-layer structures [13]. Consequently, the local climate and radiative impacts of PV rooftops in urban areas remain underexplored. In 2023, a pioneering study compared full-scale PV systems on an irrigated green roof and a bitumen roof on twin apartment blocks in Amsterdam [38]. It found that air temperatures beneath PV panels were 0.19 °C cooler at the PVIGR site compared to the PV-only site. However, the impact on air temperatures above the PV panels was not discussed. More recently, a study in Munich, Germany, examined ambient air temperature and energy balance for a non-irrigated extensive green roof and PVIGR on two residential building rooftops [39]. The PVIGR demonstrated a daytime heating effect on 2 m air temperatures of up to 1.35 °C and a nighttime cooling effect of up to 1.19 °C. These studies, however, did not include a bare roof for comprehensive comparison and were primarily conducted during summer and autumn.

Key findings from these studies indicate that PV systems increase net radiation, particularly during summer months when solar altitude is high. This additional radiation is partially converted to electricity, with the remainder dissipated as sensible heat, contributing to a localized PV heat island effect (PVHI). At night, PV panels cool rapidly, potentially lowering ambient air temperatures.

Despite these observations, a systematic comparison among bare roof, PV roof, and PVIGR systems is still lacking. The specific mechanisms by which these installations impact near-surface meteorology, such as the air temperature above and beneath PV panels and the heat conducted toward buildings, have not been thoroughly investigated. A deeper understanding of these heat exchange processes is essential for developing reliable PV parameterization schemes in urban land surface models. Furthermore, the effects of PV shading on indoor cooling and heating demands, as well as the influence of building waste heat on urban climate, require further investigation to fully understand and mitigate the UHI effect associated with PV installations.

1.3. Research objectives

While PV systems are widely recognized for their potential to reduce greenhouse gas emissions and urban energy consumption, their localized climate impacts are not well captured by current numerical climate models. This study addresses this critical gap by providing experimental insights into the local climate impacts of PV systems, which can improve PV parameterization schemes in urban land surface models. Specifically, we aim to answer the following scientific questions.

1. How do different roofing configurations (bare roof, PV roof, and PV-integrated green roofs) influence near-surface air temperatures and heat transfer into buildings?
2. What are the key factors driving the PV heat island (PVHI) effect? Can underlying plants provide cooling?
3. How can experimental findings inform the development of more accurate PV parameterization schemes in urban land surface models?

The experiment was conducted across four neighbouring rooftop sites, each approximately 200 m^2, located on a university building in subtropical Hong Kong. These sites include one bare roof, one PV roof, and two PV integrated green roof (PVIGR) sites. The study first investigates air temperature characteristics at different heights and analyses influencing factors. It then uses rooftop surface temperatures to quantify heat conduction into indoor environments, evaluating its contribution to indoor heat load. These findings can also improve PV roof configurations for heat mitigation and energy efficiency, thereby enhancing urban planning and architectural design for more sustainable development. Note that synergies between greenery and additional PV power generation are outside the scope of this research.

The paper is structured as follows: Section 2 details the experimental setups and methodology; Section 3 presents preliminary results, including the PV heating effect, influential factors, and their contributions to heat conduction into buildings; Section 4 discusses the findings and offers recommendations for developing PV parameterization schemes in urban land surface models; lastly, Section 5 provides concluding remarks.

2. Method

This section describes the study site, experimental setup, data collection, and processing methods used to investigate the impacts of different roofing configurations on urban climate and heat transfer into buildings.

Table 1
Summary of ten studies on the climate impact of PV deployment.

Ref, Year	Scale	Location	Analysis period	Key findings
[27], 2011	Small-scale, four 175W PV modules on rooftop	Portland, Oregon, USA	Sep 24–30, 2010	**Estimated sensible heat**: • PV on black roof: a negligible effect on the peak flux, but ↓total flux of 11 %. • PV on white or green roof: ↓total flux by up to 50 %, compared to black roof.
[35], 2019	Small-scale, nine 5W PV panels mounted on ground	Mesa, Arizona, USA	Few days in May–July 2018	**PV surface temperature**: • 6 °C cooler than ambient air in early morning, up to 26 °C warmer at noon. **Estimated sensible heat**: • Daytime: 80 % higher at PV site than the unshaded ground, and it shifted the peak flux to earlier hours. • Nighttime: Small negative flux from 21 p.m. to 5 a.m.
[26], 2020	Small-scale, nine 5W PV on a test building with a white roof	Tempe, Arizona, USA	Few days in Aug–Sep 2018	**Roof surface temperature**: • PV shaded roof is cooler than unshaded white roof from 9 a.m. to 3 p.m., but warmer at night. **Estimated sensible heat**: • Increase by up to 12 times (day), and around 3 times (night). **Cooling energy penalty**: • 4.9–11.2 % of PV electricity generation.
[40], 2020	Small-scale, one PV panel on a green roof	Shenzhen, China	Dec 1, 2017 to Jul 31, 2018	**PV surface temperature**: • 7.36 °C hotter than grey roof at midday, 4.03 °C cooler at midnight. **Albedo:** 0.28 (grey roof), 0.21 (grass), 0.20 (PV panel).
[37], 2018	Large-scale, PV plants on the barren ground, and a reference barren site	Gonghe, China	May 2015 to Apr 2016	**Upward shortwave radiation**: • Decrease by 5.04 % (summer), increase by 8.38 % (winter). • Computed albedo is 0.16 in summer, 0.21 in winter. **Upward longwave radiation**: • Decrease by 8.08 % in summer and 3.64 % in winter. **Net radiation**: • 8.2 % higher in summer, slightly positive in winter.
[34], 2019	Large-scale, PV plants on shrubland terrain with sandy soil, and a reference unmodified desert	Tucson, Arizona, USA	Oct 2017 to Jul 2018	**1.5 m air temperature**: • Night: No significant difference compared to reference site. • Afternoon: Average daily maximum is 1.3 °C warmer at PV sites at 3 p.m. **0.4 m air temperature**: • Night: 0.5 °C warmer. **Sensible heat flux**: • 25–50 W/m^2 higher at daytime, and slightly negative at nighttime. **Conductive heat flux**: • Daytime: 50–100 W/m^2 less downward heat flux. • Nighttime: 40–70 W/m^2 less upward heat flux.
[38], 2023	Mid-scale, PV and PVIGR on apartment rooftop	Amsterdam, Netherlands	Jun–Oct 2022	**Air temperature under PV panel**: • PVIGR site is on average 0.19 °C cooler than PV site. **Roof surface temperature under PV**:

(*continued on next page*)

Table 1 (*continued*)

Ref, Year	Scale	Location	Analysis period	Key findings
				• Daytime: PV site is 2.39 °C higher than PVIGR site. • Temperature difference increases with higher irradiation, and can reach 12 °C on a clear summer day **Power generation efficiency**: • PVIGR enhances power output by 4.4 %.
[39], 2023	Mid-scale, PVIGR and green roof on residential building rooftop	Munich, Germany	16 Jul to 30 Sep 2022	**Air temperature above PV panel**: • +1.35 °C (day), −1.19 °C (night). **Air temperature under PV panel**: • Afternoon: 3.01 °C hotter than 2 m air temperature. • Night: at most −1.44 °C cooler than reference GR. **Net radiation**: +35 W/m^2 daily. **Soil heat flux**: • Soil acts as heat sinks at daytime: 74 W/m^2 (PVIGR), −127 W/m^2 (GR). Soil releases heat at night: 40 W/m^2 (PVIGR), 60 W/m^2 (GR). • Cumulated daily is similar at around 32 Wh/m^2. **Sensible heat flux**: • Maximum difference is 204 W/m^2 (1 p.m.), −4 W/m^2 (8 p.m.). • Cumulated daily: 1477 Wh/m^2 (PVIGR), 2267 Wh/m^2 (GR). **Latent heat flux**: • Cumulated daily: 16 Wh/m^2 (PVIGR), −77 Wh/m^2 (GR).
[41]	Small-scale, one PV panel on green roof	Ljubljana, Slovenia	28 Jun to 6 Aug, and 21–28 Aug 2024	**Longwave radiation:** • Underlying GR receives up to 78 W/m^2 more than sky longwave radiation on a cloudy day, and by over 100 W/m^2 on sunny days.
[42]	Small-scale, 1 m × 0.5 m PV panel on a reduced-size model	Shenzhen, China	Aug 24–27, Dec 27–30, 2023, Jan 8–10, 2024	**External roof surface temperature**: • Bare roof is up to 22 °C (summer) and 23.9 °C (winter) higher than PV shaded roof at peak hour. **Internal roof surface temperature**: • Bare roof is up to 1.2 °C (summer) and 1.7 °C (winter) higher than PV shaded roof at peak hour. • At night, both external and internal roof surface temperatures at PV site are higher than those of bare roof in different seasons.

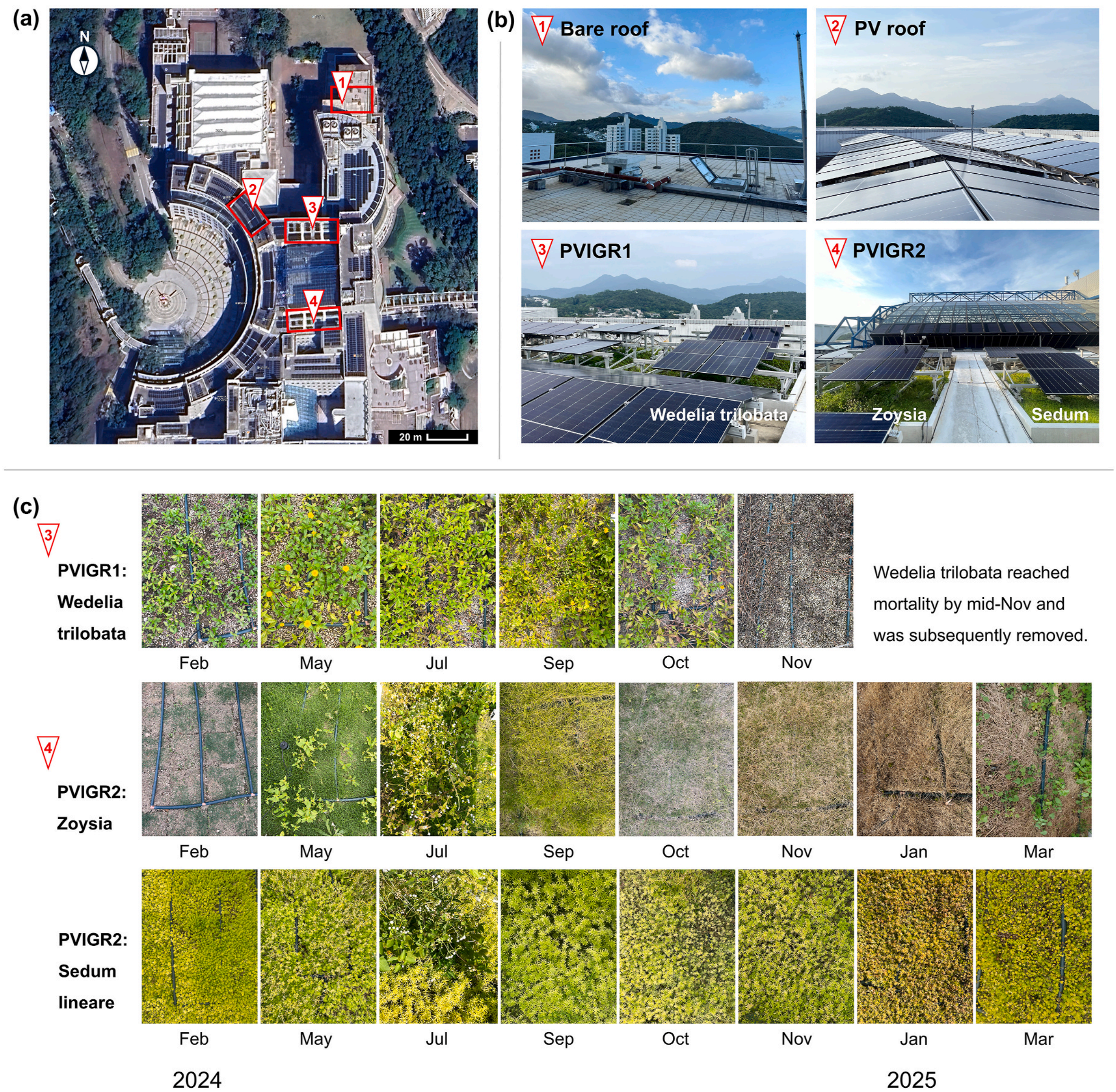

Fig. 2. (a) Site map of the four studied roofs at HKUST campus, **(b)** images of each roof, and **(c)** growth conditions of plants at two PVIGR sites from February 2024 to March 2025.

2.1. Site description

This study was conducted in Hong Kong, a coastal city in southern China characterized by a subtropical monsoon climate. The region experiences a hot and humid summer from April to November, with average air temperatures exceeding 22 °C [43]. The rainy season largely overlaps with summer, featuring occasional typhoons and thunderstorms, and contributes to an annual rainfall exceeding 2400 mm [43]. These unique climatic features make Hong Kong an ideal location for exploring effective strategies to mitigating UHI effect, particularly in cities with similar climate profiles.

The experiments were conducted at the Hong Kong University of Science and Technology (HKUST) campus located in Clear Water Bay, Hong Kong SAR, China (22.338° N, 114.264° E). Since 2020, HKUST has installed approximately 8000 solar panels on campus, generating about 3 million kWh of electricity annually. This initiative is a key component of the university's sustainability strategy, making HKUST home to one of Hong Kong's largest solar power systems and an ideal location for conducting mid-scale PV related experimental research.

Fig. 2a displays the spatial arrangement of the four monitored sites on the rooftop of a six-story academic building. The sites include a bare roof, a PV roof, and two PVIGR sites (Fig. 2b). Each site spans roughly 200 m^2 and is within a 100 m radius to ensure minimal variation in local meteorological conditions. The rooftops are free from direct anthropogenic heat sources and shading, ensuring that these factors do not significantly affect the thermal microclimate of the studied rooftops.

The PV and PVIGR sites are equipped with identical 415 W N-type Mono-crystalline solar panels from *JINKO*, with the dimension of 1855 mm × 1029 mm × 30 mm. These panels have a conversion efficiency of 21.74 % and a temperature coefficient of −0.34 %/°C under standard test conditions. Each pair of PV modules is connected to an optimizer to maximize power generation. The panels are also linked to inverters, allowing for real-time monitoring of each panel's power output every 15 min via the *SolarEdge* data platform.

As depicted in Fig. 2b (2), the PV roof site is situated on an arc-shaped roof. The panels are meticulously arranged in rows, neatly aligned like a saddle, allowing for a greater number of PV placements. Some facing southwest, while others face northeast, all tilted at a 12-degree angle from the horizontal, with a height of 0.95 m from the PV centroid to the rooftop. In contrast, the solar panels at the PVIGR1 site (Fig. 2b (3)) are installed at varying angles and heights to ensure adequate sunlight reaches the underlying vegetation. Follow

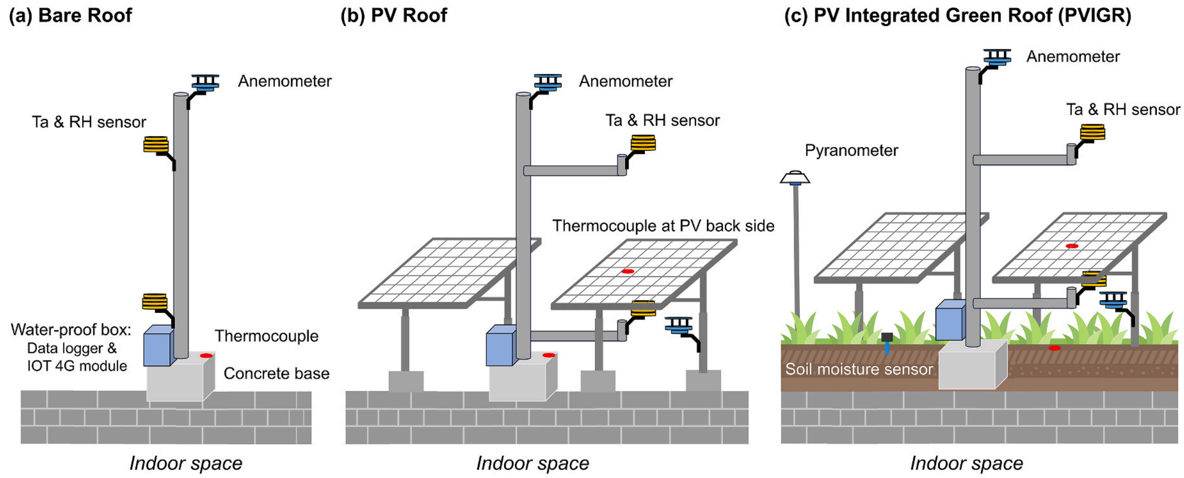

(d) Detailed information and technical specifications of the instruments

Device name	Legend	Variables	Range	Resolution	Accuracy
QTHPB Air temperature and humidity sensor		Air temperature (Ta)	-40 – 60 °C	0.1 °C	± 0.5 °C
		Relative humidity (RH)	0 – 100 %	0.5 %	± 3 %
HY-SA3E Ultrasonic anemometer		Wind Speed	0 – 70 m/s	0.1 m/s	± 3 %
		Wind Direction	0 – 359°	1°	± 3°
K-type Thermocouple		Surface temperature	-189 – 660 °C	0.1 °C	± 0.5 °C
SMP10 Pyranometer		Global horizontal irradiance	0 to 1600 W/m²	0.1 W/m²	< ±7 W/m² (at 200 W/m²)
TMO Soil moisture sensor		Soil Humidity	0 – 100 %	0.1 %	± 2 %

Fig. 3. Illustration of sensor trees at **(a)** bare roof, **(b)** PV roof, and **(c)** PVIGR sites. **(d)** Details of measurement devices.

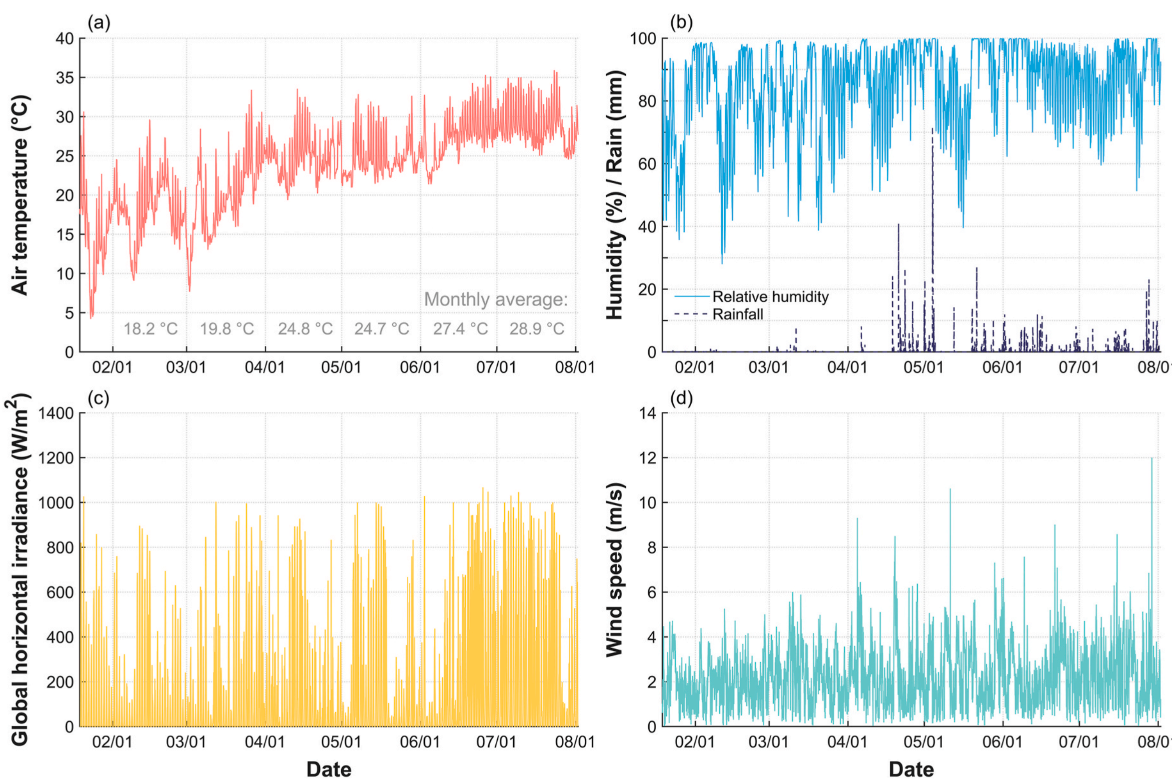

Fig. 4. Meteorological conditions from January 19 to August 1 2024, including **(a)** ambient air temperature, **(b)** relative humidity and rainfall, **(c)** global horizontal irradiance, and **(d)** wind speed. Radiation data were collected from open rooftop, while other data were sourced from a nearby automatic Supersite weather station located 1 km to the southeast of the campus, facing the coastal bay.

recommended guidelines for PVIGR [24,44], the panels are set at heights of 0.75 m, 0.9 m, and 1.05 m from the PV centroid to the soil, with a plant canopy height ranging from 0.1 to 0.4 m. All panels face south with tilt angles of 3°, 12°, and 22°. Wedelia trilobata, known for its robustness and quick ground-covering ability in warm, humid climates, was selected for its relative high evapotranspiration rate.

At the PVIGR2 site (Fig. 2b (4)), the panels are uniformly tilted at 22°, and staggered at heights of 0.75 m and 1.05 m. The vegetation consists of Zoysia on the left and Sedum linear on the right, both chosen for their drought resistance and lower irrigation needs. A white walkway runs through the centre of the rooftop, separating the two types of vegetation. Both PVIGR sites feature intensive green roofs equipped with capillary irrigation systems, which provide daily efficient and timed drip irrigation at 6–8 AM. From bottom to top, the green roof structure comprises several layers: insulation layer (5 cm), water-proofing membrane (1 mm), plastic root barrier (1 mm), plastic drainage (4 cm), geotextile filter (1 mm), lightweight growing medium (11 cm) and vegetation.

Fig. 2c details the growth conditions observed from February 2024 to March 2025. At the PVIGR1 site, Wedelia trilobata demonstrated increased density and coverage over time with minimal weed interference. The vegetation reached its peak lushness in July but began to thin out by October. By mid-November 2024, the plants showed signs of mortality due to a malfunction in the irrigation system that lasted several days, prompting the horticulture team to remove them entirely. In contrast, at the PVIGR2 site, Zoysia displayed sparse growth and desiccation during the winter months but became lush and dense by spring and summer, with a significant emergence of weeds in July. Some weeds even exceeded the height of the PV panels, necessitating trimming. The grass began to yellow in October, reached its most withered state in January 2025, and showed new sprouts by March 2025. Sedum, on the other hand, demonstrated consistent growth throughout the year, with only slight yellowing in January and a minor increase in weed presence during the summer. Overall, the plants adapted well to the capillary irrigation system, with Zoysia and Sedum demonstrating resilience throughout the year despite seasonal variations. However, the temporary malfunction in November illustrated the lower resilience of Wedelia trilobata compared to the other two plant types under irrigation disruptions.

2.2. Monitoring equipment and variables

As depicted in Fig. 3a, air temperature and humidity are monitored at 0.5 m and 1.8 m above the bare roof surface. Wind speed and direction are measured at a height of 2 m, while a thermocouple is attached to the surface of the concrete base. At the PV and PVIGR sites (Fig. 3b–c), additional thermocouples are attached to the backside of the PV panels to monitor their operational temperature. An anemometer is also installed beneath the PV panels at approximately 0.5 m to assess the airflow dynamics. Soil moisture content and temperature are measured at a depth of 0.02 m using a soil moisture sensor and a thermocouple. To measure solar radiation, a pyranometer is placed horizontally on the edge railing at PVIGR1 to record the global horizontal irradiance of the open rooftop. Note that at the PVIGR2 site, the complete sensor tree from Fig. 3c is installed on the Zoysia side, while only 0.5 m air temperature and humidity, and soil moisture sensors are deployed on the Sedum side. If not specifically mentioned otherwise, references to PVIGR2 in the following text refer to the results from the Zoysia sensor tree.

All data from these instruments are collected by data loggers and transmitted to a cloud server via Internet of Things (IoT) technology, facilitating real-time data access. Communication at the PV site is facilitated by a LoRaWAN module, while other sites utilize 4G modules for robust and efficient data transfer. Prior to deployment on the rooftops, the temperature and humidity sensors undergo calibration in a constant temperature and humidity chamber, a critical step to ensure their operational accuracy and the reliability of the data collected throughout the study. Detailed specifications and technical characteristics of all instruments are comprehensively listed in Fig. 3d.

Table 2
Physical properties of a typical bare roof and green roof construction.

Material layer	Thermal conductivity (W/mK)	Thermal resistance (m^2K/W)
25 mm Concrete tiles	1.1	0.023
20 mm asphalt	1.15	0.017
50 mm cement/sand screed	0.72	0.069
50 mm polystyrene insulation	0.034	1.471
150 mm concrete	2.16	0.069
10 mm gypsum plaster c/w white semi-gloss paint	0.38	0.026
Total (bare roof):		**1.675**
200 mm green roof layer	0.7	0.286
Total (green roof):		**1.961**

2.3. Measurement periods

The measurement instruments were installed on January 18 at the PVIGR sites, January 29 at the bare roof site, and February 4 at the PV roof site. Once installed, data collection commenced immediately and continued at 1-min intervals until March 12, 2025. Although data recording is ongoing, some sensors have experienced damage due to typhoons common in Hong Kong from late July to October. To ensure the continuity, accuracy, and comparability of data across all four sites, we primarily analysed the dataset from February to July 2024. Additionally, some useable data collected after July 2024 are visualized in the supplementary materials for reference. This half-year period effectively captures seasonal climate variations and extremes, providing insights into both hot and cold periods.

The meteorological conditions at a nearby ground-based weather station are depicted in Fig. 4. In 2024, the air temperature underwent a sharp drop from approximately 20 °C to 4.2 °C on January 23, followed by a gradual increase (Fig. 4a). Due to its coastal location, the region consistently maintained high relative humidity, exceeding 80 % each month (Fig. 4b). Rainfall became more frequent starting in April, with monthly totals of 339 mm in April, peaking at 645 mm in May, 313 mm in June, and 327 mm in July. Solar radiation showed an increasing trend, with monthly values ranging from 89,906 Wh/m^2 in February to 161,648 Wh/m^2 in July (Fig. 4c). During the summer months, southeastern winds predominated, with an average wind speed of approximately 2.2 m/s at a height of 10 m (Fig. 4d).

2.4. Data processing

Upon reviewing the raw air temperature data, we observed that for the bare roof and two PVIGR sites which utilize 4G transmission, over 94 % of data omissions consisted of missing data for just 1 min, indicating a high reliability in the data transmission at these sites. Specifically, the bare roof and PVIGR2 sites experienced only one instance where missing data exceeded 60 min. Conversely, at the PV site where LoRaWAN module technology is used for data transmission, there were 18 instances of data missing for periods longer than 60 min, highlighting a lesser reliability compared to 4G technology.

For processing missing data, linear interpolation was applied to gaps shorter than 60 min to maintain data continuity. In cases where data gaps exceeded 60 min, the missing values were left as "NaN" to ensure the integrity of the analysis. Data visualization was primarily conducted using hourly averages. Additionally, Pearson correlation tests were conducted to explore the relationships among various variables, crucial for understanding the interdependencies and influencing factors among the monitored variables.

In Section 3.5, we apply Fourier's law to estimate the heat

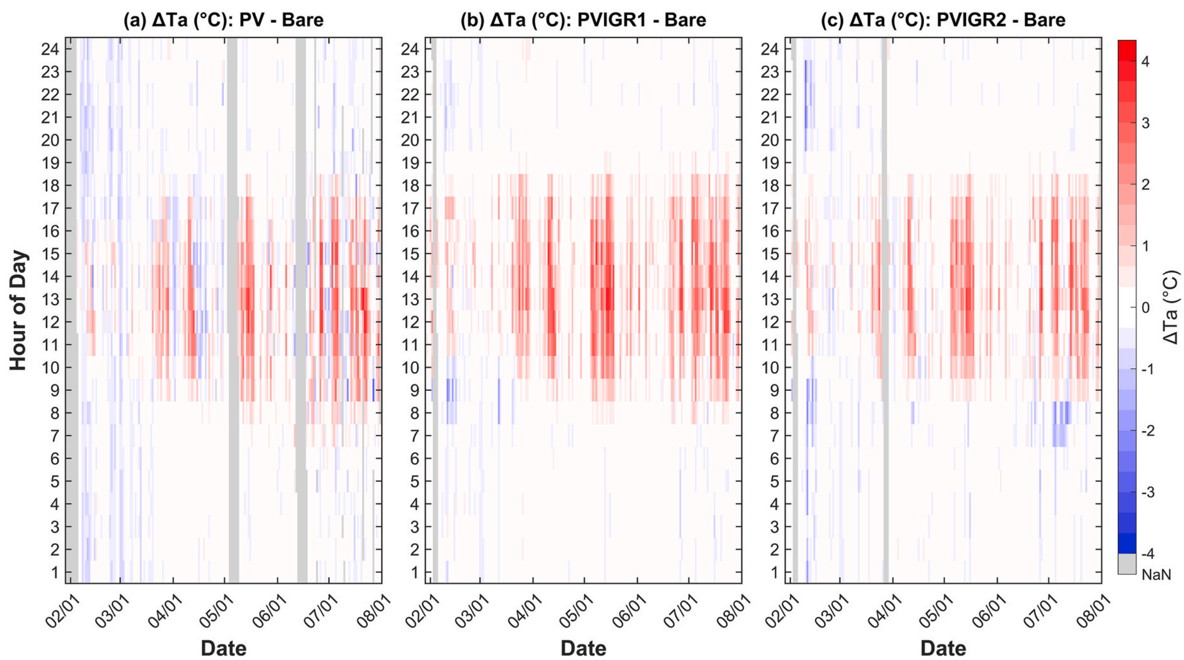

Fig. 5. Hourly air temperature difference between **(a)** PV site, **(b)** PVIGR1 site, and **(c)** PVIGR2 site, compared to the bare roof site, from January 29 to August 1. Grey areas represent periods with missing data (NaN).

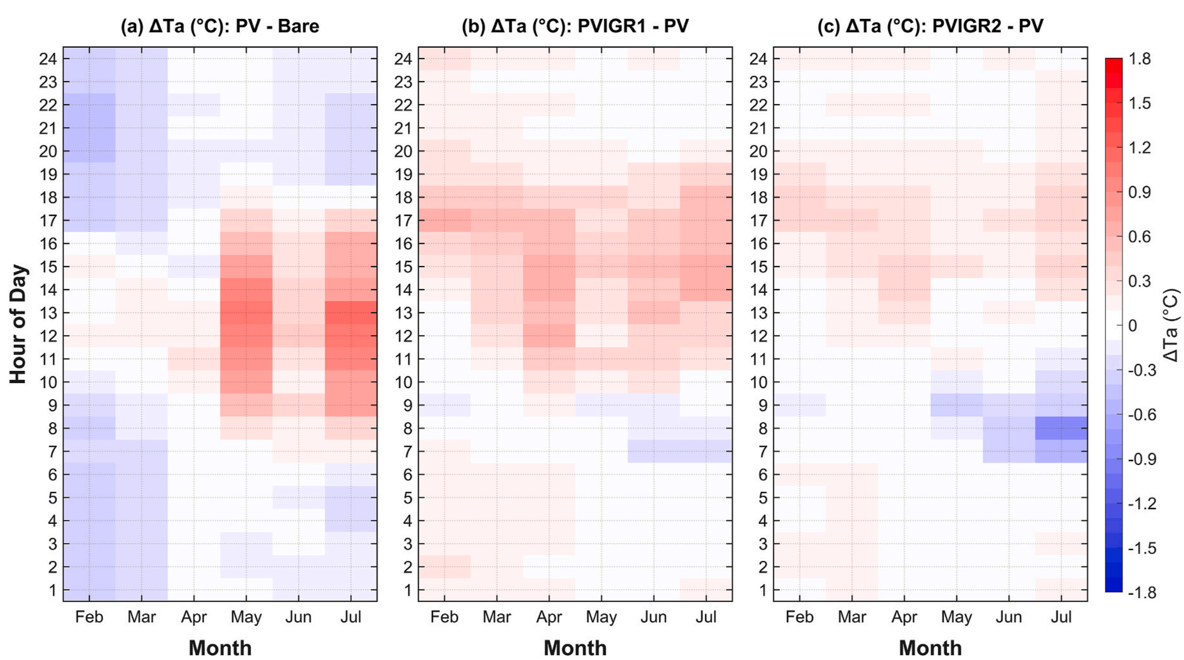

Fig. 6. Monthly averages of hourly air temperature differences (ΔTa) between **(a)** PV roof and bare roof, **(b)** PVIGR1 and PV roof, and **(c)** PVIGR2 and PV roof. Data analysis is confined to periods without any missing data (NaN), ensuring accuracy and reliability of the observed trends among groups. For detailed hourly air temperature differences, refer to Fig. S1 in the supplementary materials.

conduction from each roof type to the interior of the building, expressed as Eq. (1):

$$Q_{cond} = \frac{kA\Delta T}{d}. \quad \text{Eq. (1)}$$

where, Q_{cond} is the conductive heat flux (W), k is the thermal conductivity of the material (W/mK), A is the area of the roof (m^2), ΔT is the temperature difference between two adjacent layers (K), and d is the thickness of each layer of the material (m).

After integrating each layer's contribution, the conductive heat flux per unit area of each roof configuration can be calculated as Eq. (2):

$$\frac{Q_{cond}}{A} = \frac{T_R - T_B}{R_{total}}, \quad \text{Eq. (2)}$$

$$R_{total} = \sum \frac{d_i}{k_i}. \quad \text{Eq. (3)}$$

where, T_R is the measured rooftop surface temperature, T_B is the fixed temperature of 25 °C as the indoor boundary condition. R_{total} is the total thermal resistance for a multilayer roof (m^{2}K/W), calculated the sum of each layer's individual resistances.

According to Hong Kong building design standard [45], a typical roof construction in Hong Kong is listed in Table 2. At PVIGR site, the measured T_R is at the soil surface at 0.02 m depth. The average thickness of soil and substrate is 0.2 m, with conductivity is 0.7 W/mK [46]. Thus, we set the total thermal resistance of PVIGR configuration to 1.818 m^2K/W, compared to 1.675 m^2K/W of the default roof settings at bare roof and PV roof sites.

3. Results

3.1. Heating effect of PV panels at 1.8 m

To quantify the thermal impact of PV panels on the air at 1.8 m, Fig. 5 illustrates the heating effect at PV and PVIGR sites compared to a bare roof site from January 29 to August 1 2024. During daylight hours (7 a.m.–6 p.m.), the solar panels exhibit a noticeable heating effect on the overlying air, particularly pronounced starting from May. The most significant temperature differences were observed during the noon hour (12 p.m.), reaching peak values of 3.82 °C on Jul 21, 3.96 °C on May 14, and 3.48 °C on May 14 at the PV, PVIGR1, and PVIGR2 sites, respectively. Notably, the 15-min average air temperature difference at the PV site can reach as high as 5.16 °C, indicating a substantial localized warming effect. This intense heat is significant, especially when walking on the rooftop. During nighttime, the PV panels typically show a slight cooling effect, generally less than 1 °C. The greatest cooling effects recorded are −2.72 °C on Jul 27, −2.09 °C on Feb 11, and −2.67 °C on Feb 10 at the PV, PVIGR1, and PVIGR2 sites, respectively. This finding contrasts with the notable annual nighttime warming of 3.5 °C observed in solar power plants located in desert environment, compared to nearby bare desert [13].

To explore broader trends, Fig. 6 presents monthly averages of hourly air temperature differences (ΔTa) between PV and bare roofs, clarifying seasonal variations. During the colder months of February and March, daytime temperature differences are minimal, generally under 0.2 °C. This slight heating effect can be attributed to lower solar angles and higher albedo in winter [37], which reduce solar energy absorption by PV panels. As the months warm up, these differences become more pronounced, peaking at 1.06 °C in May and 1.18 °C in July (Fig. 6a), indicative of a significant photovoltaic heat island (PVHI) effect. In contrast, the nighttime cooling effect is more substantial during winter, with the maximum reduction observed in February at −0.46 °C, which declines to −0.24 °C by July.

Fig. 6b and c presents the air temperature differences between the PVIGR sites and the standard PV site. Both PVIGR sites exhibit a slight warming effect, except during the morning hours from 6 to 9 a.m., which align with the irrigation schedule. This pattern is consistent throughout the year, as shown in the supplementary materials (Fig. S1), where full-year hourly air temperature differences are provided. Notably, the warming is particularly pronounced in the afternoon, with increase of 0.6 °C at PVIGR1 and 0.3 °C at PVIGR2. Surprisingly, the PVIGR sites did not demonstrate a cooling effect at the 1.8 m height, a finding that merits further discussion.

As indicated by Ref. [14], the PV mounting style significantly affects heat convection from the panel to the air and the radiative exchange with the surrounding environment, illustrating how physical configurations impact microclimatic conditions. This relationship is further explored in urban land surface models, where variations in PV arrangements are captured by integrating 'roughness length' as a critical factor [34,47]. Roughness length plays a significant role in the dynamics of momentum and heat exchange between the roof and the air [48–51], linking atmospheric processes with physical surface characteristics [52].

At the PVIGR1 site, diverse heights and tilt angles of the PV panels contribute to a more complex surface geometry, likely resulting in a larger roughness length that enhances turbulent air mixing and improves heat dissipation [53,54]. This observation aligns with prior

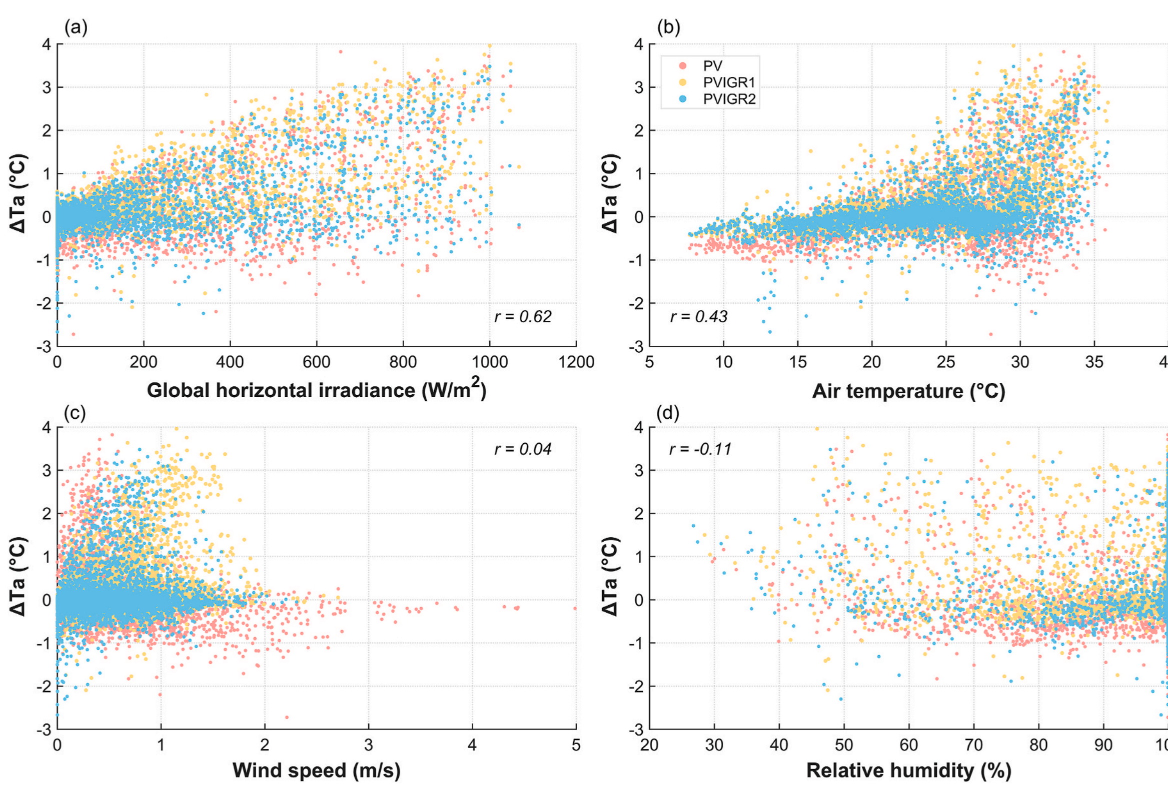

Fig. 7. Relationship between hourly air temperature difference (ΔTa) of each site relative to the bare roof and various environmental factors, including **(a)** rooftop solar irradiance, **(b)** ambient air temperature from Supersite weather station, **(c)** wind speed at each site, and **(d)** relative humidity at each site. r represents the Pearson correlation coefficient. Data collected over the six-month measurement period.

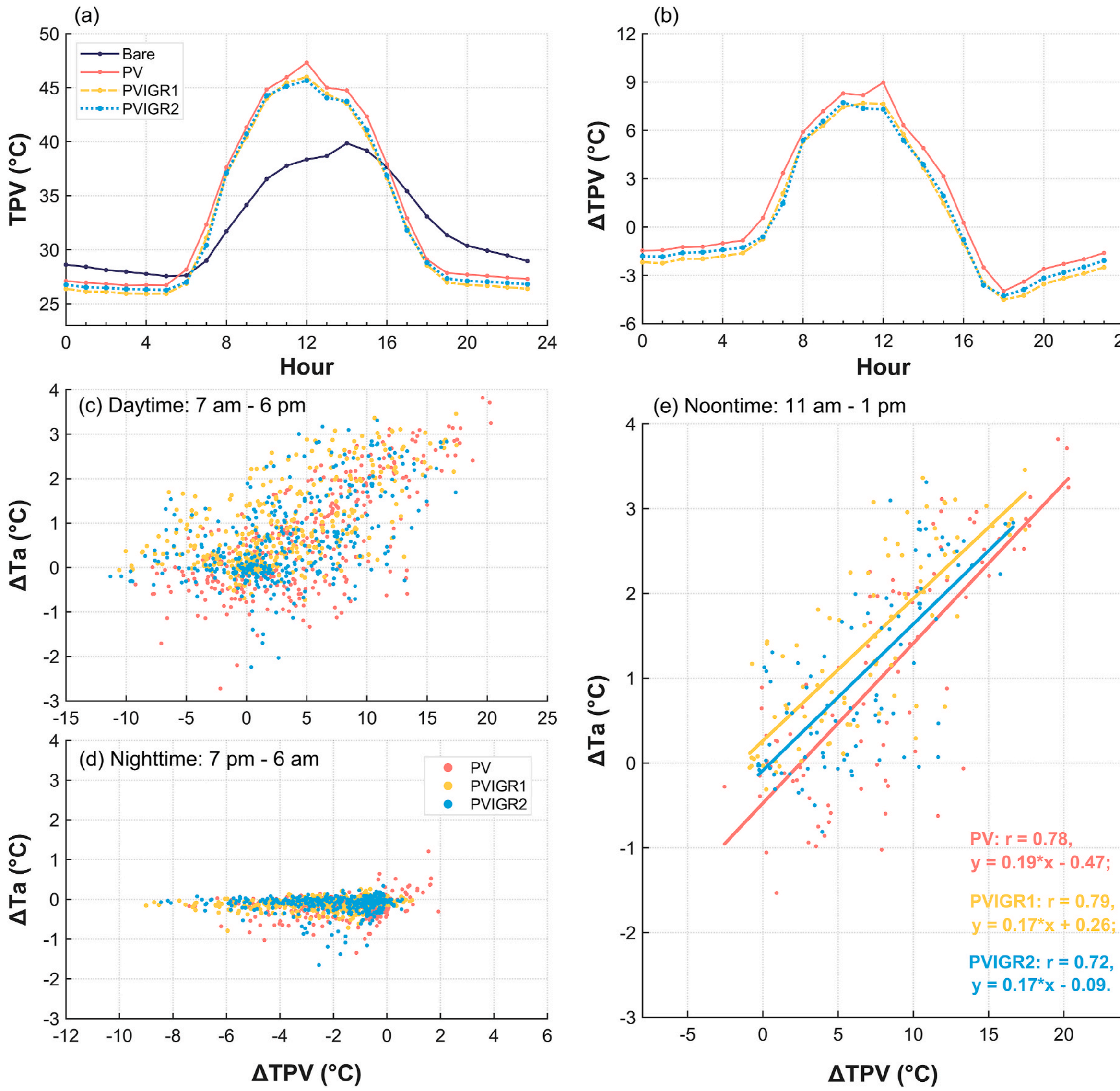

Fig. 8. (a) Monthly average diurnal profile of PV surface temperature (TPV) variations at PV roof, PIVGR1, and PVIGR2 sites in July, alongside the concrete surface temperature of bare roof as a reference. **(b)** Surface temperature difference (ΔTPV) for the PV roof, PVIGR1, and PVIGR2, relative to the bare roof. Correlation between the surface temperature difference (ΔTPV) and the air temperature difference (ΔTa) relative to the bare roof at each site during: **(c)** Daytime: 7 a.m.–6 p.m., **(d)** Nighttime: 7 p.m.–6 a.m., and **(e)** Noontime: 11 a.m.–1 p.m., including linear regression lines and equations.

research [34], which suggests that increased surface roughness, due to drag and associated wake production by PV modules, facilitates more efficient upward transport of sensible heat during the day. Conversely, the PVIGR2 site, with more uniform panel arrangements at the same tilt angles but varying heights, exhibits a slightly simpler geometry and a lower roughness length than PVIGR1, though still higher than that of the standard PV site. The PV site, featuring panels neatly aligned in a saddle shape, displays low surface roughness length, leading to higher horizontal wind speed but reduced vertical turbulence.

3.2. Cause of PV heating effect at 1.8 m

In Section 3.1, we observed significant variations in the PV heating effect above PV panels, particularly the pronounced temperature increases during warmer months and the differing impacts across PV sites. These findings highlight the complexity of the PV heating phenomenon, underscoring the need to understand the specific environmental factors driving these temperature dynamics.

Fig. 7 illustrates the relationships between the hourly air temperature difference (ΔTa) and various environmental factors, including irradiance, air temperature, wind speed, and relative humidity. Data from three sites (PV, PVIGR1, PVIGR2) were analysed, revealing remarkably similar trends. Pearson correlation coefficients (r) and other statistical results were calculated using data from all sites to ensure robustness. The p-values for all correlations were extremely small ($p < 0.001$), confirming the statistical significance of the observed relationships.

Fig. 7a shows a moderate to strong positive correlation ($r = 0.62$) between irradiance and ΔTa. Higher irradiance levels lead to increased PVHI intensity, with a maximum increase of 4 °C observed at 1000 W/m^2. The linear regression model, $\Delta Ta = 0.0018 \times \text{irradiance} - 0.1096$, explains 39 % of the variance (coefficient of determination $R^2 = 0.39$). Fig. 7b displays a positive trend in ΔTa as ambient air temperature increases, with $r = 0.43$. The warming effect is more pronounced on hotter days (consistent with the findings in Ref. [34]), sometimes exceeding 2.0 °C when air temperatures rise above 24 °C.

In contrast, the correlation between wind speed and PVHI intensity is very weak (Fig. 7c, $r = 0.04$), with the highest PVHI typically observed at lower wind speeds (0–1 m/s). This suggests that higher wind speeds help disperse heat, thus reducing localized warming effects. This effect is more pronounced at the PV site, where lower roughness length and occasionally higher wind speeds reduce the warming effect compared to PVIGR sites (as shown in Fig. 6b and c). Fig. 7d reveals a weak negative correlation between relative humidity and PVHI ($r = -0.11$), indicating that humidity levels have limited influence on the PV heating effect.

The data in Fig. 7 are based on hourly averages throughout the day. Analysis of specific time periods — daytime (7 a.m.–6 p.m.) and noontime (12–2 p.m.) — align with the overall daily trend. However, nocturnal data (7 p.m.–6 a.m.) show a slight cooling effect, with an average reduction of −0.11 °C (Fig. S2b). Lower ambient air temperatures are associated with greater PV cooling effects at night ($r = 0.36$). By analysing these correlations, we identified irradiance as the most significant factor influencing the PV heating effect, followed by ambient air temperature. Wind speed and relative humidity have lesser impacts on PVHI.

Furthermore, PV installations absorb solar radiation, leading to higher PV surface temperatures (TPV) which can heat the surrounding air through convection. This effect potentially contributes to a localized PV heat island phenomenon. Fig. 8a displays the monthly average diurnal profile of TPV for various roofing types during July, the month with the highest solar radiation and temperatures. TPV rises quickly after sunrise and remains higher than the surface temperature of bare roof from 7 a.m. to 3 p.m. Notably, the peak TPV reaches 47.32 °C at 12 p.m., while the peak temperature on the bare roof is 39.85 °C at 2 p.m., resulting in a maximum temperature difference of 8.97 °C at 12 p.m. (Fig. 8b).

Conversely, PVIGRs mitigate peak temperatures, reducing them by 1.33 °C for PVIGR1 and 1.66 °C for PVIGR2 compared to the PV roof. After 4 p.m., PV surfaces cool more rapidly than bare roof, with the most significant temperature difference of approximately 4 °C occurring at 6 p.m. At night, the lower heat capacity of PV panels facilitates faster release of stored heat, leading to temperatures that are 1–3 °C cooler than those of bare roof. This phenomenon persists even in November, as illustrated in Fig. S3. Compared to the PV site, the average nighttime cooling effect is enhanced at the PVIGR sites, with reductions of 0.90 °C at PVIGR1 and 0.62 °C at PVIGR2.

Further analysis revealed correlations between the difference in PV panel surface temperature and bare roof surface temperature (ΔTPV) and the air temperature difference (ΔTa) relative to the bare roof at each site, as detailed in Fig. 8c for daytime, Fig. 8d for nighttime, and Fig. 8e for noontime. During daytime, ΔTPV exhibits a positive correlation with ΔTa, with correlation coefficients (r) at each site all greater than 0.5, indicating that higher PV surface temperatures relative to the bare roof generally correspond with increased PVHI intensity at the PV sites. This relationship is especially strong at noon (Fig. 8e), where all three sites exhibit correlation coefficients above 0.7, indicating a very strong positive correlation. The steeper slope observed at the PV site compared to the PVIGR sites suggests that the plants in PVIGRs may indirectly contribute to a cooling effect. At night, the correlation becomes less pronounced, with r values smaller than 0.2.

3.3. Heating effect of PV panels at 0.5 m

After examining the heating effects above PV panels, this section focuses on the air temperature under PV panels (Ta_{under}) to understand the dynamics of near-surface temperatures. As indicated in Fig. S4a and Fig. 9a, both daily and monthly average hourly results consistently show that Ta_{under} at the PV site is generally higher than at the bare roof site, particularly during daytime. Specifically, the hourly air temperature under PV panels can reach up to 4.86 °C higher than at the bare roof site at noon on July 22 (Fig. S4a). The monthly averages of hourly air temperature differences (ΔTa_{under}) peak at noon, reaching 0.92 °C, 0.80 °C, 0.40 °C, 1.26 °C, 0.85 °C, and 1.64 °C from February to July, respectively. The intensity of the PV-induced heat island effect under the panels surpasses that observed above the panels, as illustrated in Fig. 6a.

At night, however, the heating effect is minimal, averaging 0.09 °C, typically ranging from 0 to 0.2 °C. This minimal nighttime heating effect is contributed by two mechanisms: 1) the reduced sky view factor under the PV canopy, which impedes longwave radiative cooling and traps heat; 2) the shading provided by the PV panels during the day, which reduces heat absorption by the underlying concrete roof, resulting in less heat release at night [34].

At the PVIGR sites, Ta_{under} during the daytime remains slightly higher than at the bare roof site, as shown in Figs. S4b–d. However, results from Fig. 9b–d and Fig. S5 indicate that, compared to the PV site, the plants at PVIGR sites contribute to cooling at this height. Among the

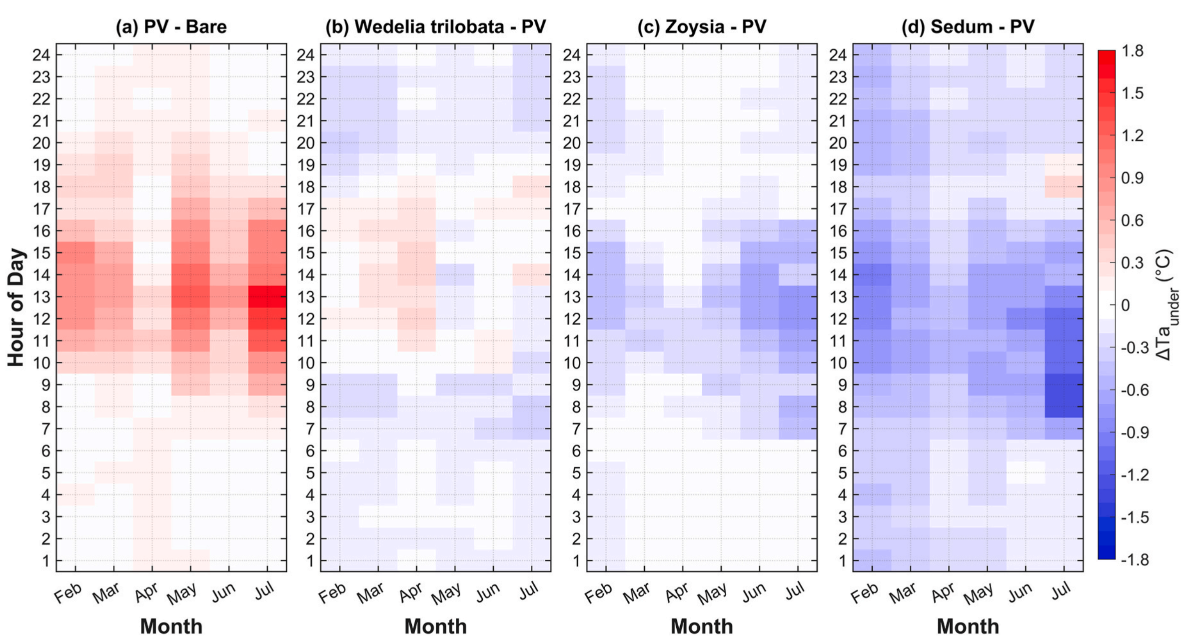

Fig. 9. Monthly averages of hourly air temperature differences under PV panels (ΔTa_{under}) for **(a)** PV roof versus bare roof, **(b)** Wedelia trilobata (at PVIGR1) versus PV roof, **(c)** Zoysia (at PVIGR2) versus PV roof, and **(d)** Sedum (at PVIGR2) versus PV roof. Analysis excludes periods with missing data (NaN).

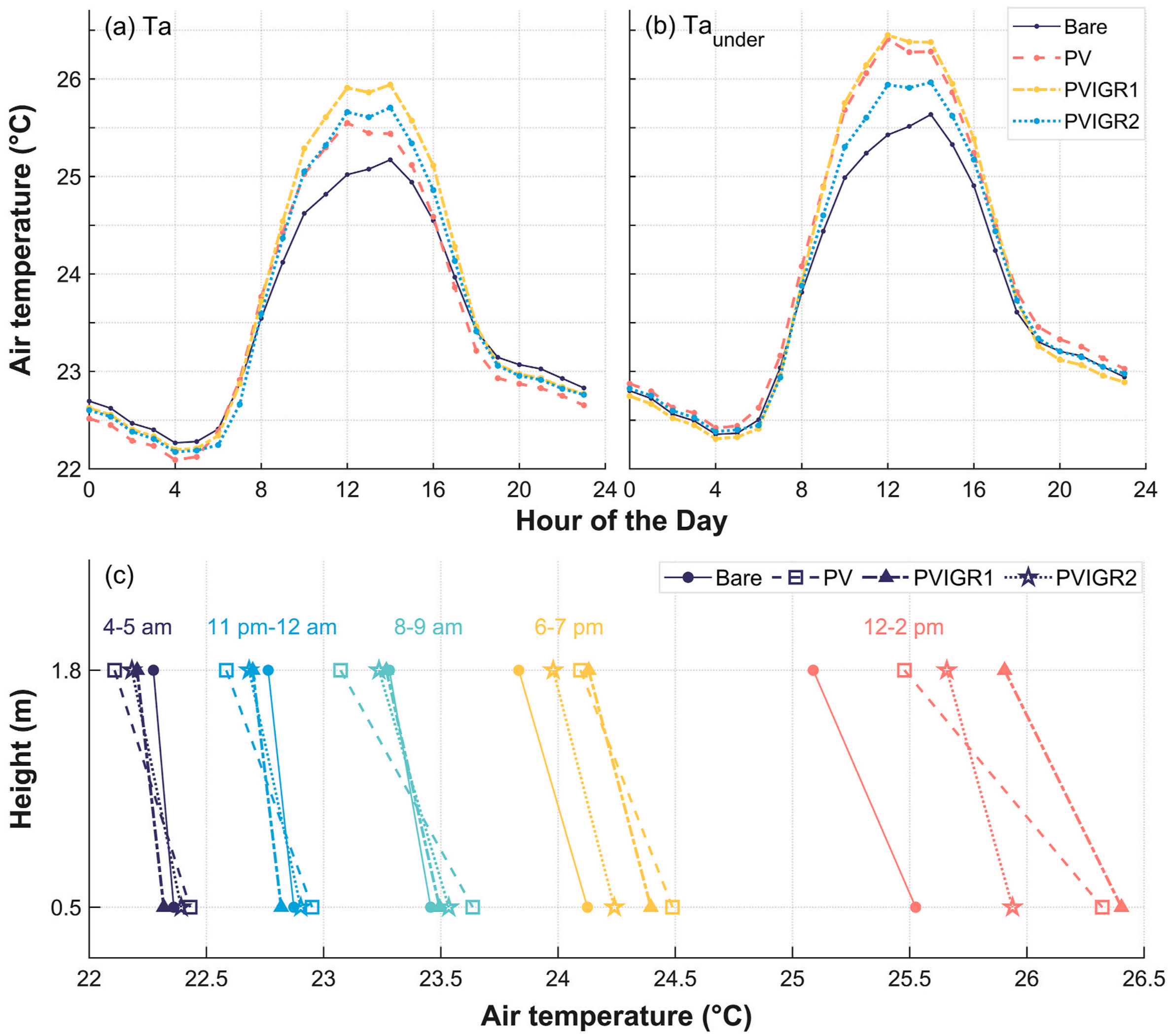

Fig. 10. Average diurnal profiles of air temperature **(a)** above PV panels at 1.8 m height (Ta), and **(b)** under PV panels at 0.5 m height (Ta_{under}). **(c)** Average Ta and Ta_{under} over five distinct periods of the day, color-coded by local time. Line styles indicate different sites: solid for Bare roof, dashed for PV roof, dash-dot for PVIGR1, and dotted for PVIGR2 site (Zoysia). Analysis covers the entire measurement period, excluding missing data (NaN). (For interpretation of the references to color in this figure legend, the reader is referred to the Web version of this article.)

three studied species, Sedum at PVIGR2 site has the strongest cooling effect throughout the day (Fig. 9d), with average reductions of −0.55, −0.43, −0.27, −0.37, −0.34, and −0.44 °C from February to July. The largest cooling intensity exceeds −1 °C in the morning in July, peaking at −1.26 °C at 8 a.m. As shown in Fig. 9c, Zoysia also displays a pronounced cooling effect during the day, with a maximum reduction of 0.77 °C at noon in July. At night, Wedelia trilobata at PVIGR1 exhibits better cooling effects, ranging from 0.1 to 0.4 °C (Fig. 9b). While plant transpiration contributes to cooling, this effect may also be influenced by the arrangement of PV panels at PVIGR1, as noted by Broadbent et al. [34]. This setup likely enhances heat dissipation and reduces heat trapping by increasing surface roughness and promoting turbulent mixing, resulting in cooler air temperatures beneath the panels.

We then analyse the average diurnal profiles of air temperatures at different heights. As depicted in Fig. 10a, the air temperature at a height of 1.8 m (Ta) at the bare roof site remains the lowest from 8 a.m. to 4 p.m., peaking at 25.17 °C at 2 p.m. In contrast, the peak temperatures at the PV and two PVIGR sites occur between 12 p.m. and 2 p.m., reaching 25.55 °C, 25.94 °C, and 25.71 °C respectively. This suggests that PV installations on rooftops may lead to both an earlier and higher peak in urban temperatures. After 7 p.m., the bare roof site becomes the warmest due to heat release, extending the warming effect until 6 a.m. Although Ta over the PV site is the coldest at night, the temperature under the PV panels (Ta_{under}) is the highest among all sites (Fig. 10b), indicating a significant PV-canopy heating effect.

To further explore the PV-canopy heating effect, we calculate the average air temperatures at heights of 0.5 m and 1.8 m during five critical time steps throughout the measurement period: 1) the coldest time from 4:00 to 5:59, 2) the hottest time from 12:00 to 14:59, 3) midnight from 23:00 to 00:59, 4) morning from 8:00 to 9:59, and 5) evening from 18:00 to 19:59.

As illustrated in Fig. 10c, the steepness of the lines connecting the measurements at 1.8 m and 0.5 m heights correlates with the temperature differences between these levels. A more vertical line indicates a smaller temperature difference. The PV site consistently exhibits the largest temperature differences (Ta_{under} – Ta) across all periods, peaking at 0.84 °C between 12 and 2 PM. In comparison, the temperature differences are 0.44 °C at the bare roof site, 0.50 °C at the PVIGR1 site, and 0.28 °C at the PVIGR2 site. This highlights a significant PV-canopy heating effect at sites with neatly arranged PV panels, which restricts heat dissipation and traps heat beneath them, creating a warmer microclimate underneath. Conversely, this effect is somewhat mitigated at the PVIGR sites, likely due to the combined influences of plant evaporative cooling and less uniform PV panel arrangements. These

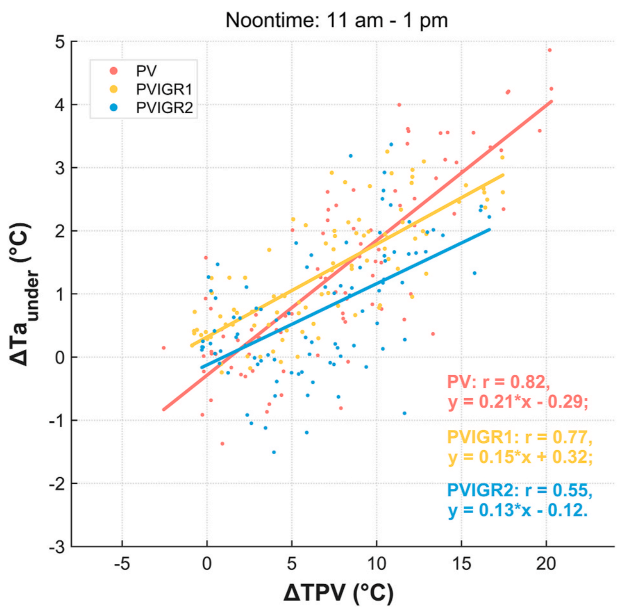

Fig. 11. Similar to Fig. 8e, but for ΔTa_{under}. Correlation between surface temperature difference (ΔTPV) and ΔTa_{under} relative to the bare roof at each site at noontime: 11 a.m. – 1 p.m., including linear regression lines and equations.

factors help moderate the microclimate by enhancing heat dispersion and cooling through evapotranspiration.

3.4. Cause of heating effect at 0.5 m

In this section, we explore the mechanisms behind the heating effects observed beneath PV panels, particularly the significant midday heating shown in Fig. 10. PV panels, operating at elevated surface temperatures in hot environments, can experience reduced efficiency due to these thermal conditions. Understanding the causes of the PV-canopy heating effect is crucial for optimizing system design and mitigating adverse thermal impacts.

As depicted in Fig. 11, at the PV site, there is a strong positive correlation between the change in PV surface temperature (ΔTPV, compared to the surface temperature of the bare roof) and the change in air temperature under PV panels (ΔTa_{under}, compared to the 0.5 m height air temperature at the bare roof site), with a correlation coefficient (r) of 0.82. The linear regression model, $\Delta Ta_{under} = 0.21 \times \Delta TPV - 0.29$, suggests that increases in TPV significantly influence the air temperature under PV panels. When PV panels operate at elevated temperatures, they emit substantial longwave radiation downward, consistent with previous findings that the received longwave radiation below PV panels can be up to 100 W/m^2 (equivalent to over 20 %) higher than under clear sky [41]. The orderly arrangement of PV panels reduces the sky view factor, impeding longwave radiative cooling and intensifying the heating effect.

When comparing the PV site with two PVIGR sites, the linear regression models show slopes of 0.15 and 0.13 for PVIGR sites, with r values of 0.77 and 0.55, respectively. These results suggest that Ta_{under} at PVIGR sites is less sensitive to changes in TPV, indicating that plants moderate the warming impact. Consequently, the presence of plants not only helps alleviate the intensification of the thermal environment caused by PV panels, but also indirectly enhances the panels' power generation efficiency by maintaining cooler operational conditions. Although this aspect is beyond the scope of the current study, preliminary analyses indicate a potential efficiency increase due to the cooler thermal conditions beneath the PV canopies.

Green roofs cool the air primarily through the released of latent heat via surface evapotranspiration. Thus, the cooling effectiveness is expected to be greatly influenced by soil moisture content, which represents the evaporative potential of the land surface. However, our research shows a surprisingly weak correlation between soil moisture and cooling effects during daytime across three plant species (Fig. 12a), with a correlation coefficient (r) of only 0.07. Interestingly, at night, higher soil moisture content is associated with reduced cooling (r = 0.26), as shown in Fig. 12b. This phenomenon can be attributed to the increased heat capacity of the irrigated soil, which stores heat during the day and releases it at night via soil heat conduction [40,55], partially offsetting the cooling effect of the grass roof.

In humid regions like Hong Kong, our findings indicate that soil moisture has a marginal impact on evapotranspiration and the associated cooling effects, aligning with a previous experimental study in Hong Kong [56]. Consequently, the cooling efficiency of green roofs, in such humid environments, relies less on water availability and more on energy availability. This contrasts sharply with arid regions, where limited water availability directly restricts evapotranspiration [57,58]. Our findings suggest that in humid climates, other factors such as solar radiation and air temperature might have a more significant impact on cooling [59,60].

Fig. 12c and d reveal that the cooling effect of plants moderately correlates with solar irradiance and ambient air temperature, with r values of −0.43 and −0.32, respectively. This suggests that higher levels of solar irradiance and warmer temperatures generally enhance evapotranspiration and promote photosynthesis, consistent with previous findings [59]. Notably, the Sedum species is particularly sensitive to solar radiation (r = −0.59), possibly due to its lighter appearance and higher albedo, which help reflect sunlight. In contrast, Zoysia is more responsive to air temperature (r = −0.44), indicating enhanced cooling efficacy under warmer conditions.

Intense wind can improve heat and water vapor transport, thereby enhancing the evapotranspiration rate [60]. As shown in Fig. 12e, lower wind speeds are associated with more significant cooling effects (more negative ΔTa_{under}), suggesting that in calm conditions, the cooling effect is more pronounced. This observation might be due to reduced heat convection in low wind scenarios, allowing the area beneath panels to remain cooler. Conversely, higher wind speeds seem to transport the cooler air to downstream.

Continuous vaporization of water through evapotranspiration leads the air above the soil surface to become gradually saturated. As indicated by relative humidity ranging from 80 % to 100 % in Fig. 12f, the environment approaches saturation, which could suppress further evapotranspiration, aligning with our previous discussions. Sedum, in particular, demonstrates superior water retention capabilities by maintaining very high relative humidity levels near saturation. This efficiency in retaining moisture, evidenced by soil moisture measurements that are 33 % higher than Zoysia and 29 % higher than Wedelia trilobata under identical watering conditions, highlights its distinct advantage over the other species studied.

3.5. Roof surface temperature and heat conduction

The installation of PV panels on rooftops provides shading to the underlying concrete, significantly reducing the conductive heat flux into buildings. We examined the roof surface temperature (TR) at different sites, including the concrete surface temperature of the bare roof, beneath PV panels at the PV site, and the soil surface temperature at the PVIGR1 site. These measurements (Fig. 13a and b) are crucial for calculating the conductive heat flux towards buildings (Fig. 13c and d), assuming a fixed indoor boundary conditions of 25 °C as detailed in Section 2.4.

To assess performance under varied climate conditions, we selected three consecutive sunny and rainy days. On July 23–25 (Fig. 13a), during one of the hottest sunny periods without rain, the temperature on the bare roof peaked at 48.75 °C at 2 p.m. on July 23, which was

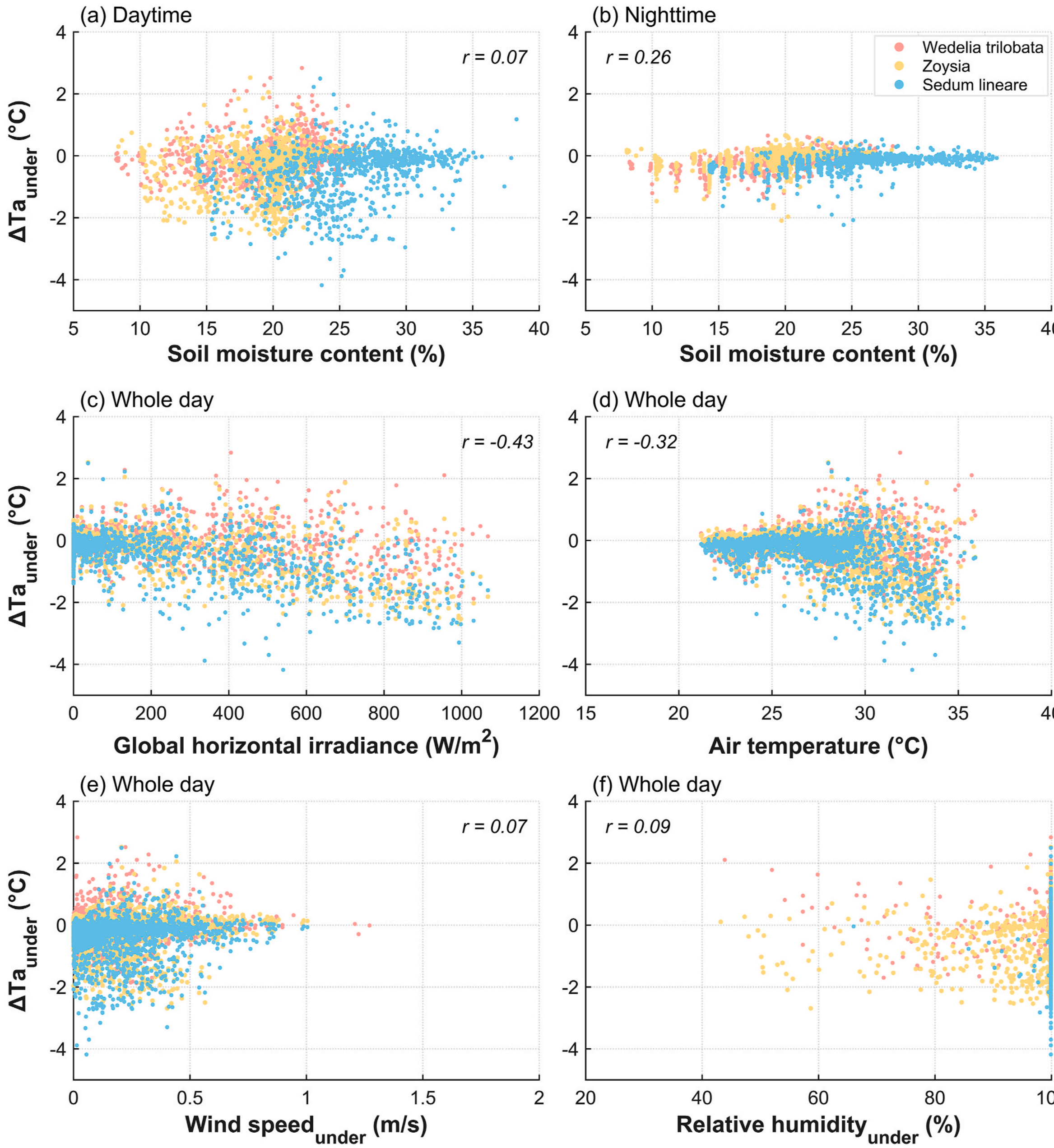

Fig. 12. Relationship between hourly air temperature difference (ΔTa_{under}) of PVIGR sites compared to PV roof and various environmental factors, including **(a)** soil moisture content during daytime, **(b)** soil moisture content during nighttime, **(c)** solar irradiance, **(d)** ambient air temperature (from Supersite weather station), **(e)** wind speed under PV panels at each site, and **(f)** relative humidity under PV panels at each site. ***r*** represents the correlation coefficient. Data from May 1 to July 31.

14.10 °C and 15.22 °C higher than at the PV and PVIGR sites, respectively. Over the next two days, the temperature difference was around 10 °C. PV panels provided significant shading, limiting the peak temperature at the PV site to 35.43 °C. At night, TR at the PV site was occasionally up to 1 °C higher than at the bare roof site, due to impeded radiative cooling. The PVIGR site consistently maintained soil surface temperatures about 0.90 °C lower than the PV site over this period.

On July 28, a heavy rain day with 82.6 mm of accumulated rainfall, TR across different rooftops was very similar (Fig. 13b), with the maximum temperature difference being only 1.61 °C cooler at the PV site compared to the bare roof. During July 29–30, which had cumulative rainfall of only 3.0 and 14.5 mm, the temperature differences remained below 10 °C. On these rainy days, TR at the PVIGR site was on average 0.44 °C higher than at the PV site. These observations are consistent with previous research [56], suggesting that increased soil moisture from rainfall enhances thermal insulation and inhibits downward heat transfer. This promotes heat accumulation near the surface, resulting in warmer substrate temperatures. Conversely, on sunny days, increased evapotranspiration tends to lower soil surface temperatures.

As conductive heat flux towards buildings is highly correlated with roof surface temperature, we calculated the daily cumulative heat conduction for three different roof types, as illustrated in Fig. 13c and d. From July 23 to 25, the PV site demonstrated significant reductions in daily heat conduction compared to the bare roof: with decreases of 45.7 %, 33.8 %, and 32.0 % respectively. At the PVIGR site, which incorporates a green roof for enhanced thermal insulation, reductions were even more substantial at 60.6 %, 52.8 %, and 49.7 %. The cumulative heat conduction over these three days was 0.42 kWh/m^2 for the bare roof, 0.26 kWh/m^2 for the PV roof, and 0.19 kWh/m^2 for the PVIGR site. These values represent reductions of 37.6 % and 54.6 % for the PV

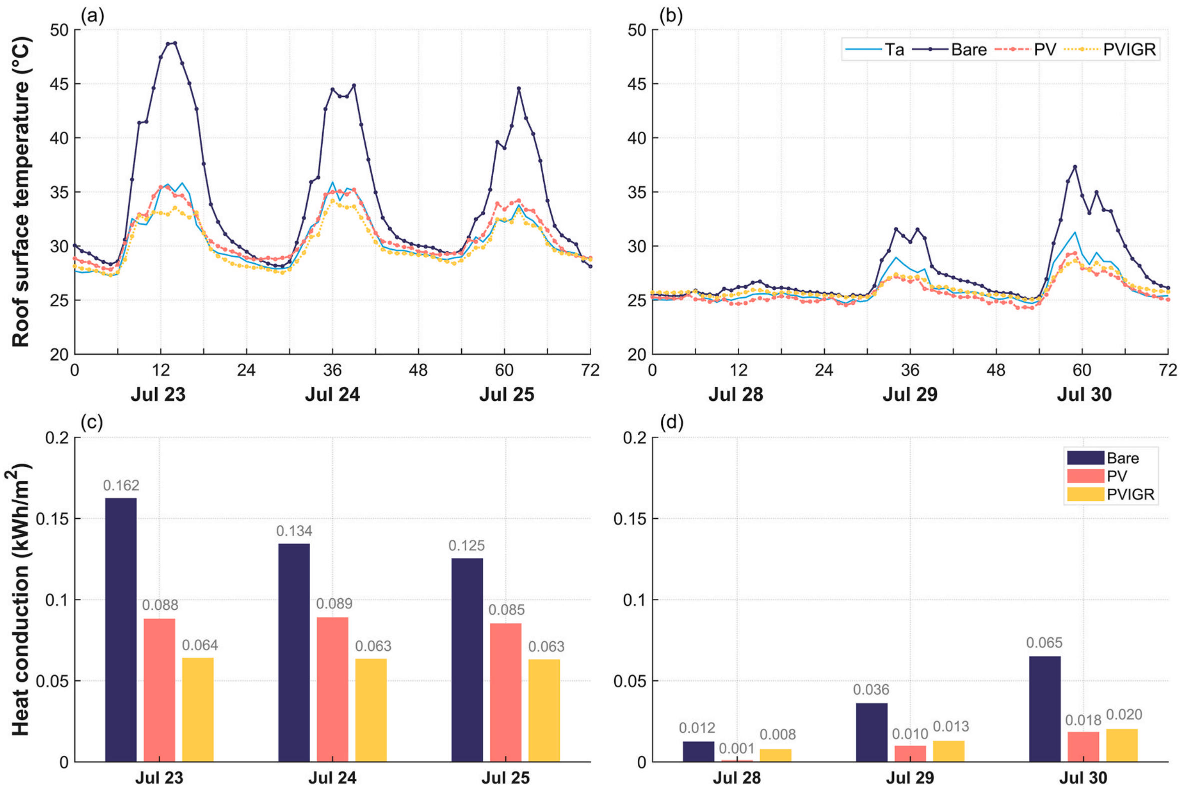

Fig. 13. Diurnal variations of roof surface temperature (TR) during **(a)** sunny days (July 23–25) and **(b)** rainy days (July 28–30), with ambient air temperature (Ta) from the Supersite weather station provided for reference. Daily heat conduction into indoor space on **(c)** sunny days (July 23–25) and **(d)** rainy days (July 28–30), respectively.

and PVIGR sites respectively, highlighting the effectiveness of PV installations in reducing cooling demands during hot and sunny conditions.

On rainy days, the observed heat conduction values for the bare roof were 0.012 kWh/m^2, 0.036 kWh/m^2, and 0.065 kWh/m^2, consecutively. Summing up three days, the PV roof achieved a 74.6 % reduction in heat conduction compared to the bare roof, while the PVIGR setup exhibited a significant decrease of 64.0 %. These observations underscore the thermal insulation benefits provided by both PV and PVIGR installations, suggesting their potential to significantly reduce indoor cooling demands and enhance energy efficiency in building designs.

4. Discussion

This study conducted comprehensive full-scale measurements to assess the climate impact of bare roof, PV roof, and two PVIGR sites. The half-year observations provided valuable insights into the complex physical processes occurring across different roof configurations. These findings can be parameterized into urban land surface models and coupled with the numerical climate models, such as the Weather Research and Forecasting model (WRF) [61,62] and the Community Earth System Model (CESM) [63,64].

4.1. Insights for urban land surface modelling

Compared to conventional bare roof, all PV-installed rooftops exhibited daytime warming at 1.8 m height, with PV heat island (PVHI) intensity peaking under conditions of high solar irradiance and ambient temperatures. These results contradict modelling studies that suggest PV systems mitigate urban warming using the "effective albedo" method [28,30]. Such approaches oversimplify PV energy exchanges by treating them as equivalent to roofing material with an effective albedo (summing panel conversion efficiency and solar reflectance). This method often predicts cooling effect when the effective albedo exceeds the background environment albedo [28–30]. While some studies using darkened albedo values report surface warming [65,66], these parameterizations still fail to capture the distinct diurnal temperature profiles of PV surfaces, substantial midday sensible heat flux contributions, and pronounced vertical microclimate stratification beneath PV canopies. As noted by Ref. [14], the "effective albedo" based approach cannot represent real-world PV climate impacts, but may misdirect urban heat mitigation strategies.

Recent modelling advances have attempted more physically realistic representations of PV systems. Masson et al. [31] introduced a PV scheme in the Town Energy Balance model that simulated daytime UHI reduction (0.2 °C), but relied on the problematic assumption that PV back surface temperatures equal ambient air temperatures. Our measurements, consistent with Phoenix observations [67], recorded panel temperatures exceeding 65 °C at noon, invalidating this assumption and its derived sensible heat flux estimates [31,32]. More sophisticated parameterization in WRF/BEP + BEM [33] better reproduce observed diurnal patterns (daytime warming with slight nighttime cooling), but may incorrectly treat all sensible heat flux as upward emissions. Our data reveal significant heat retention beneath PV panels, with PV canopy air temperatures averaging 0.86 °C warmer at noon than above-panel measurements over six months. This PV-canopy heating effect stems from three mechanisms: **(1)** thermal emissions from heated PV panels warming trapped air through convection and radiation; **(2)** reduced sky view factor limiting longwave radiative cooling; and **(3)** restricted airflow inhibiting heat dissipation under the canopy.

The accurate representation of sensible heat flux is crucial for evaluating PV climate impacts in numerical climate models, as PV panels convert substantial solar energy into convective heat [34]. While recent studies consider convective heat transfer from both front and back panel surfaces, assuming upward transport [27,33,68,69], the notable heat retention beneath PV canopy suggests that a substantial portion of this heat does not escape upwards as previously estimated. Field measurements confirm this complexity, showing approximately 10 % higher sensible heat fluxes at PV sites during peak hours compared to reference locations [34]. Furthermore, during July, PVIGR exhibited a cooling effect of up to −1.26 °C beneath the panels (Fig. 9), a phenomenon not observed above the panels (Fig. 6). These findings highlight the importance of microclimatic interactions within the PV canopy. Conventional upward flux assumptions may overestimate atmospheric heating and exaggerate PVHI intensity, while underestimating near-surface thermal effects.

Additionally, the microclimatic impacts of PV systems are further modulated by array configuration, which critically governs energy exchange processes [14,70]. Ordered PV arrangements exacerbate PV-canopy heating through reduced surface roughness and limited sky view factor, whereas irregular layouts with varied panel heights and angles promote turbulent mixing that helps dissipate trapped heat. This configuration-dependent behaviour highlights the need for more refined representations of PV systems in parameterization scheme.

Beyond atmospheric interactions, PV installations significantly alter building thermal dynamics through shading effects. Our measurements show PV roof reduced heat conduction by 37.6 % over three consecutive clear days in July, with PVIGR achieving 54.6 % reductions through combined shading and enhanced insulation. While winter heating penalties occur, these remain negligible in Hong Kong's mild and short winters. More importantly, the resulting reduction in air conditioning demand creates a positive feedback loop by decreasing waste heat emissions - ultimately mitigating UHI intensity and further reducing cooling loads [6,71,72]. These complex PV-energy-climate interactions necessitate integrated modelling approaches that combine building energy simulations with urban canopy models.

Thus, to enable accurate large-scale assessments of PV impacts, we emphasize two critical modelling advancements.

1) **Reasonable PV parameterization schemes**: It is crucial to consider surface roughness length and PV-canopy heating effects. Influenced by PV array configuration and mounting geometry, these factors significantly alter both above- and below-canopy air temperatures, and system energy balances.
2) **Integration of BEM with urban canopy models**: This allows for a more comprehensive analysis of PV impact, from direct microclimate modification to indirect effects through altered building energy use and subsequent waste heat patterns.

The reliability of previous modelling studies that suggested PV roofs produce cooling effects in hot and sunny days remains questionable, unless they consider: (1) site-specific parameter settings, (2) PV-induced reductions in building energy demand (including waste heat emissions), and/or (3) associated displacement of fossil fuel consumption. While coupled modelling framework, such as WRF/BEP + BEM [33], BEM + CM [73,74], BEM + SLUCM [63,75,76], have shown promise, rigorous validation against field measurements remains essential. We suggest a two-stage evaluation framework to comprehensively assess PV impacts: First, isolate direct climatic effects through simulations excluding building energy use; second, incorporate building energy feedback mechanisms to quantify indirect effects, particularly the modulation of air conditioning waste heat on urban microclimates [71,77]. This systematic approach will provide policymakers with more reliable assessments of PV systems' climate impacts.

4.2. Lessons learned from experimental design

While our observations clearly reveal the impacts of PV panel on local meteorological conditions, there is room for improvement in the design of future experiments.

To ensure comparability between different sites, it is crucial to select locations away from natural surfaces, nearby structures, and anthropogenic heat sources, such as A/C outdoor units. However, site selection might be constrained by factors like building security requirements, which can limit the available options for ideal experimental conditions. For example, in our study, the arrangement of PV panels at the PV and PVIGR sites differed due to site selection limitations. This variation in panel layout, combined with the presence of plants, may have influenced the observed temperature effects. Although we analysed the underlying causes of these differences, the potential confounding factors highlight the need for further research in more controlled settings.

Moreover, our results identified significant warming at a height of 1.8 m due to PV installations. It would be valuable to explore whether this warming effect extends to higher altitudes, as previous studies suggest that thermal energy dissipates completely above 10 m [34,78]. Unfortunately, the Hong Kong Lands Department enforces a maximum height of 2.5 m for rooftop systems, which restricts our ability to explore thermal effects at greater heights and prevents the installation of advanced instruments such as ultrasonic eddy covariance towers for detailed turbulent heat transport analysis.

Additionally, the accuracy of results heavily depends on the quality of in-situ measurements. Sensors should be installed at the same height, and the sensor tree should be positioned centrally on the PV rooftop to avoid edge effects. The downwind portion of a PV array can be warmer than upwind due to horizontal advection, as shown by Fthenakis and Yu [78] using computational fluid dynamics (CFD) calculations.

Furthermore, reliable data transmission via IoT technology is essential. We selected LoRaWAN for its energy efficiency, intending to power the sensor tree with PV panels instead of direct wiring. We chose 4G for its maturity and reliability, despite its higher power consumption. However, LoRaWAN experienced data loss issues due to limited gateway availability, making 4G the more reliable option in our experiment.

Finally, our study involved an intensive green roof with an irrigation system managed by the campus management office. While we knew the timing of the automatic irrigation system, the precise quantity was not documented, limiting our exploration of soil water balance. Future studies should document these aspects, and PV-integrated non-irrigated extensive green roofs are worth exploring.

5. Conclusions

This study presents the first real-world scale measurement of the photovoltaic (PV) impact on urban climate, conducted across four rooftop sites on a university campus in a subtropical region. The configurations compared include a bare roof, a PV roof, and two PV integrated green roofs (PVIGR), each covering approximately 200 m^2.

Our six-month field measurements reveal that different roof configurations significantly affect the local microclimate. At night, PV panels induced a slight cooling effect compared to the bare roof, reducing temperatures by up to −2.72 °C hourly and −0.46 °C on a monthly average basis. Conversely, during the daytime, both PV and PVIGR sites exhibited localized warming above the panels, with temperature increases reaching up to 4 °C at noon on sunny days. This warming, known as the PV heat island (PHVI) effect, was notably pronounced during warmer months, with monthly average temperature differences of 0.3 °C in February and 1.3 °C in July at noon. Correlation analysis identified PV panel surface temperature, solar irradiance, and ambient air temperatures as the primary drivers of the PVHI effect. The peak surface temperatures of PV panels, characterized by their low albedo, low emissivity, and low heat capacity, were higher and occurred earlier than those of the bare roof, shifting peak air temperatures from 2 p.m. to between 12 p.m. and 2 p.m. This shift in peak temperatures, resulting from widespread rooftop PV deployment, could significantly influence urban energy demand and peak loads patterns, necessitating further investigation.

In contrast to the PV roof, the PVIGR configuration did not exhibit a cooling effect above the panels, likely due to the humid subtropical climate of Hong Kong, which may constrain the evaporative cooling potential of plants. Additionally, the placement of PV panels might facilitate turbulent heat mixing, diminishing their cooling potential at a height of 1.8 m. However, beneath the panels, plants significantly reduced air temperatures by up to 1.26 °C during July mornings. This not only mitigates under-panel heating but may potentially enhance PV efficiency by lowering panel surface temperatures by more than 1 °C. Among the plant species investigated, Sedum stood out as particularly effective, making it a preferable choice due to its lower water requirements and higher albedo.

Moreover, both PV and PVIGR demonstrated promise in reducing heat transfer into buildings, a critical benefit for cities with predominant cooling demands. This reduction in cooling load further decreases waste heat emitted by air conditioning, thereby contributing to the mitigation of the urban heat island effect—an outcome that, while not directly measurable in-situ, can be effectively modelled using advanced urban land surface models. In light of these findings, we advocate for specific refinements in modelling methodologies for future research, particularly incorporating factors such as PV-canopy heating effects and surface roughness, which are influenced by panel arrangement [34,37,47]. The integration of building energy models with urban canopy models is necessary to comprehensively assess the climatic impacts of widespread PV deployment.

Notably, some studies found that the potential global mean PV-induced warming is much smaller compared to the expected climate change from fossil fuel combustion [30,79–81]. While this study focuses on the local climate impacts of PV systems, the broader benefits of PV deployment—such as reducing greenhouse gas emissions and mitigating global climate change—remain significant. Our findings can also inform strategies for optimizing PV systems to minimize local warming effects while maximizing their global climate benefits.

In conclusion, while the evapotranspiration capacity of plants in humid climates may be constrained, their cooling ability under PV panels is crucial. This not only helps mitigate the PVHI effect but also improves PV efficiency and reduces building cooling requirements. Additionally, green roofs support stormwater management, aligning with initiatives for developing sponge city. Future studies should explore PV integrated green roofs with and without irrigation, investigate the impacts of integrating PV with white roofs, the impacts of dust accumulation on PV performance and associated thermal effects [82], and expand the scope to diverse climatic zones [20]. These explorations could deepen our understanding of these technologies and enhance their applications in urban environments.

CRediT authorship contribution statement

Liutao Chen: Conceptualization, Methodology, Data curation, Validation, Formal analysis, Investigation, Writing – original draft, Writing – review & editing, Visualization. **Zinan Lin:** Investigation, Resources, Validation, Project administration. **Qi Zhou:** Investigation, Resources, Visualization. **Shihong Zhang:** Investigation, Resources. **Mengying Li:** Writing – review & editing, Supervision. **Zhe Wang:** Writing – review & editing, Supervision, Funding acquisition.

Declaration of competing interest

The authors declare that they have no known competing financial interests or personal relationships that could have appeared to influence the work reported in this paper.

Acknowledgement

The work described in this paper is supported by a grant from the Research Grants Council of the Hong Kong Special Administrative Region, China (Project No. C6003-22Y). We thank to the help from Davis BOOKHART and Marcus Leung-Shea from HKUST Sustainability/Net-Zero Office. We also want to thank Mr. Wicky Lee for providing his practical experience when selecting the plants.

Appendix A. Supplementary material

Supplementary material to this article can be found online at https://doi.org/10.1016/j.rser.2025.115709.

Data availability

The data in this study are available from Dr. Liutao Chen (chenlt@ust.hk) upon reasonable request.

References

[1] Oke TR, Mills G, Christen A, Voogt JA. Urban climates. Cambridge university press; 2017.
[2] Huang WTK, Masselot P, Bou-Zeid E, Fatichi S, Paschalis A, Sun T, et al. Economic valuation of temperature-related mortality attributed to urban heat islands in European cities. Nat Commun 2023;14:7438.
[3] Ho JY, Shi Y, Lau KK, Ng EY, Ren C, Goggins WB. Urban heat island effect-related mortality under extreme heat and non-extreme heat scenarios: a 2010–2019 case study in Hong Kong. Sci Total Environ 2023;858:159791.
[4] Santamouris M, Cartalis C, Synnefa A, Kolokotsa D. On the impact of urban heat island and global warming on the power demand and electricity consumption of buildings—A review. Energy Build 2015;98:119–24.
[5] Li X, Zhou Y, Yu S, Jia G, Li H, Li W. Urban heat island impacts on building energy consumption: a review of approaches and findings. Energy 2019;174:407–19.
[6] Kikegawa Y, Nakajima K, Takane Y, Ohashi Y, Ihara T. A quantification of classic but unquantified positive feedback effects in the urban-building-energy-climate system. Appl Energy 2022;307:118227.
[7] Kikegawa Y, Tanaka A, Ohashi Y, Ihara T, Shigeta Y. Observed and simulated sensitivities of summertime urban surface air temperatures to anthropogenic heat in downtown areas of two Japanese major cities, Tokyo and Osaka. Theor Appl Climatol 2014;117:175–93.
[8] Santamouris M. Cooling the Cities–A review of reflective and green roof mitigation technologies to fight heat island and improve comfort in urban environments. Sol Energy 2014;103:682–703.
[9] Yang J, Wang Z-H, Kaloush KE. Environmental impacts of reflective materials: is high albedo a 'silver bullet' for mitigating urban heat island? Renew Sustain Energy Rev 2015;47:830–43.
[10] Ban-Weiss G, Wray C, Delp W, Ly P, Akbari H, Levinson R. Electricity production and cooling energy savings from installation of a building-integrated photovoltaic roof on an office building. Energy Build 2013;56:210–20.
[11] Dehwah AH, Asif M. Assessment of net energy contribution to buildings by rooftop photovoltaic systems in hot-humid climates. Renew Energy 2019;131:1288–99.
[12] Kapsalis V, Maduta C, Skandalos N, Wang M, Bhuvad SS, D'Agostino D, et al. Critical assessment of large-scale rooftop photovoltaics deployment in the global urban environment. Renew Sustain Energy Rev 2024;189:114005.
[13] Barron-Gafford GA, Minor RL, Allen NA, Cronin AD, Brooks AE, Pavao-Zuckerman MA. The photovoltaic heat Island effect: larger solar power plants increase local temperatures. Sci Rep 2016;6:35070.
[14] Sailor D, Anand J, King R. Photovoltaics in the built environment: a critical review. Energy Build 2021;253:111479.
[15] Hasanuzzaman M, Malek A, Islam M, Pandey A, Rahim N. Global advancement of cooling technologies for PV systems: a review. Sol Energy 2016;137:25–45.
[16] Köhler M, Schmidt M, Laar M, Wachsmann U, Krauter S. Photovoltaic panels on greened roofs. Rio 2002;2:151–8.
[17] Zhang Y, Chen T, Gasparri E, Lucchi E. A modular agrivoltaics building envelope integrating thin-film photovoltaics and hydroponic urban farming systems: a circular design approach with the multi-objective optimization of energy, light, water and structure. Sustainability 2025;17:666.
[18] Wang W, Yang H, Xiang C. Green roofs and facades with integrated photovoltaic system for zero energy eco-friendly building–A review. Sustain Energy Technol Assess 2023;60:103426.
[19] Abdalazeem ME, Hassan H, Asawa T, Mahmoud H. Review on integrated photovoltaic-green roof solutions on urban and energy-efficient buildings in hot climate. Sustain Cities Soc 2022;82:103919.
[20] Talwar P, Verma N, Khatri H, Ahire PD, Chaudhary G, Lindenberger C, et al. A systematic review of photovoltaic-green roof systems in different climatic conditions focusing on sustainable cities and societies. Sustain Cities Soc 2023:104813.
[21] Lamnatou C, Chemisana D. A critical analysis of factors affecting photovoltaic-green roof performance. Renew Sustain Energy Rev 2015;43:264–80.
[22] Houchmand LJ, Martí MM, Gassó-Domingo S. Photovoltaics and green roofs: holistic analysis in built environments. Renew Sustain Energy Rev 2025;207:114987.
[23] Vijayaraghavan K. Green roofs: a critical review on the role of components, benefits, limitations and trends. Renew Sustain Energy Rev 2016;57:740–52.
[24] Osma-Pinto G, Ordóñez-Plata G. Measuring factors influencing performance of rooftop PV panels in warm tropical climates. Sol Energy 2019;185:112–23.

[25] He Y, Hii D, Wong N. Solar photovoltaics deployment impact on urban temperature: review and assessment recommendations. Build Environ 2024: 111920.
[26] Brown KE, Baniassadi A, Pham JV, Sailor DJ, Phelan PE. Effects of rooftop photovoltaics on building cooling demand and sensible heat flux into the environment for an installation on a white roof. J Eng Sustain Build Cities 2020;1: 021001.
[27] Scherba A, Sailor DJ, Rosenstiel TN, Wamser CC. Modeling impacts of roof reflectivity, integrated photovoltaic panels and green roof systems on sensible heat flux into the urban environment. Build Environ 2011;46:2542–51.
[28] Taha H. The potential for air-temperature impact from large-scale deployment of solar photovoltaic arrays in urban areas. Sol Energy 2013;91:358–67.
[29] Ma S, Goldstein M, Pitman A, Haghdadi N, MacGill I. Pricing the urban cooling benefits of solar panel deployment in Sydney, Australia. Sci Rep 2017;7:43938.
[30] Hu A, Levis S, Meehl GA, Han W, Washington WM, Oleson KW, et al. Impact of solar panels on global climate. Nat Clim Change 2016;6:290–4.
[31] Masson V, Bonhomme M, Salagnac J-L, Briottet X, Lemonsu A. Solar panels reduce both global warming and urban heat island. Front Environ Sci 2014;2:14.
[32] Salamanca F, Georgescu M, Mahalov A, Moustaoui M, Martilli A. Citywide impacts of cool roof and rooftop solar photovoltaic deployment on near-surface air temperature and cooling energy demand. Boundary-Layer Meteorol 2016;161: 203–21.
[33] Zonato A, Martilli A, Gutierrez E, Chen F, He C, Barlage M, et al. Exploring the effects of rooftop mitigation strategies on urban temperatures and energy consumption. J Geophys Res Atmos 2021;126:e2021JD035002.
[34] Broadbent AM, Krayenhoff ES, Georgescu M, Sailor DJ. The observed effects of utility-scale photovoltaics on near-surface air temperature and energy balance. J Appl Meteorol Climatol 2019;58:989–1006.
[35] Pham JV, Baniassadi A, Brown KE, Heusinger J, Sailor DJ. Comparing photovoltaic and reflective shade surfaces in the urban environment: effects on surface sensible heat flux and pedestrian thermal comfort. Urban Clim 2019;29:100500.
[36] Hernandez RR, Easter S, Murphy-Mariscal ML, Maestre FT, Tavassoli M, Allen EB, et al. Environmental impacts of utility-scale solar energy. Renew Sustain Energy Rev 2014;29:766–79.
[37] Chang R, Shen Y, Luo Y, Wang B, Yang Z, Guo P. Observed surface radiation and temperature impacts from the large-scale deployment of photovoltaics in the barren area of Gonghe, China. Renew Energy 2018;118:131–7.
[38] van der Roest E, Voeten JG, Cirkel DG. Increasing solar panel output with blue-green roofs in water-circular and nature inclusive urban development. Build Environ 2023;244:110704.
[39] Fassbender E, Pytlik S, Rott J, Hemmerle C. Impacts of rooftop photovoltaics on the urban thermal microclimate: metrological investigations. Buildings 2023;13:2339.
[40] Chen X, Jeong S, Zheng Y, Park H, Park CE, Joo J, et al. Evaluation of different roof materials for the mitigation of urban warming in a subtropical monsoon climate. J Geophys Res Atmos 2020;125:e2019JD031972.
[41] Žižak T, Medved S, Arkar C. Effect of solar photovoltaics on green roof energy balance and evapotranspiration. Sustain Cities Soc 2025;121:106206.
[42] He Y, Yang Z, Fan Y. Thermal performance analysis for roofs with heat mitigation strategies in subtropical hot and humid regions. Sci Rep 2025;15:6117.
[43] Observatory HK. Monthly Meteorol Normal Hong Kong (1991-2020) 2021.
[44] Shafique M, Luo X, Zuo J. Photovoltaic-green roofs: a review of benefits, limitations, and trends. Sol Energy 2020;202:485–97.
[45] (EMSD) EMSD. Guidelines on performance-based building energy code. Hong Kong: EMSD; 2007.
[46] Ouldboukhitine S-E, Belarbi R, Djedjig R. Characterization of green roof components: measurements of thermal and hydrological properties. Build Environ 2012;56:78–85.
[47] Chang R, Luo Y, Zhu R. Simulated local climatic impacts of large-scale photovoltaics over the barren area of Qinghai, China. Renew Energy 2020;145: 478–89.
[48] Masson V, Grimmond CSB, Oke TR. Evaluation of the town energy balance (TEB) scheme with direct measurements from dry districts in two cities. J Appl Meteorol 2002;41:1011–26.
[49] Masson V. A physically-based scheme for the urban energy budget in atmospheric models. Boundary-Layer Meteorol 2000;94:357–97.
[50] Mascart P, Noilhan J, Giordani H. A modified parameterization of flux-profile relationships in the surface layer using different roughness length values for heat and momentum. Boundary-Layer Meteorol 1995;72:331–44.
[51] Martilli A, Clappier A, Rotach MW. An urban surface exchange parameterisation for mesoscale models. Boundary-Layer Meteorol 2002;104:261–304.
[52] Kanda M, Kanega M, Kawai T, Moriwaki R, Sugawara H. Roughness lengths for momentum and heat derived from outdoor urban scale models. J Appl Meteorol Climatol 2007;46:1067–79.
[53] Chen L, Yang J, Li P. Modelling the effect of BIPV window in the built environment: uncertainty and sensitivity. Build Environ 2022;208:108605.
[54] Macdonald R, Griffiths R, Hall D. An improved method for the estimation of surface roughness of obstacle arrays. Atmos Environ 1998;32:1857–64.
[55] Chen X, Jeong S-J. Irrigation enhances local warming with greater nocturnal warming effects than daytime cooling effects. Environ Res Lett 2018;13:024005.
[56] Jim CY, Peng LL. Substrate moisture effect on water balance and thermal regime of a tropical extensive green roof. Ecol Eng 2012;47:9–23.
[57] Jamei E, Chau HW, Seyedmahmoudian M, Stojcevski A. Review on the cooling potential of green roofs in different climates. Sci Total Environ 2021;791:148407.
[58] Solcerova A, van de Ven F, Wang M, Rijsdijk M, van de Giesen N. Do green roofs cool the air? Build Environ 2017;111:249–55.
[59] Jim CY, Tsang S. Ecological energetics of tropical intensive green roof. Energy Build 2011;43:2696–704.
[60] Cascone S, Coma J, Gagliano A, Pérez G. The evapotranspiration process in green roofs: a review. Build Environ 2019;147:337–55.
[61] Yang J, Wang Z-H, Chen F, Miao S, Tewari M, Voogt JA, et al. Enhancing hydrologic modelling in the coupled weather research and forecasting–urban modelling system. Boundary-Layer Meteorol 2015;155:87–109.
[62] Chen F, Kusaka H, Bornstein R, Ching J, Grossman-Clarke S, Loridan T, et al. The integrated WRF/urban modeling system: development, evaluation, and applications to urban environmental problems 2011.
[63] Li XC, Zhao L, Oleson K, Zhou Y, Qin Y, Zhang K, et al. Enhancing urban climate-energy modeling in the community earth system model (CESM) through explicit representation of urban air-conditioning adoption. J Adv Model Earth Syst 2024; 16:e2023MS004107.
[64] Oleson K, Feddema J. Parameterization and surface data improvements and new capabilities for the community land model urban (CLMU). J Adv Model Earth Syst 2020;12:e2018MS001586.
[65] Millstein D, Menon S. Regional climate consequences of large-scale cool roof and photovoltaic arraydeployment. Environ Res Lett 2011;6:034001.
[66] Li Y, Kalnay E, Motesharrei S, Rivas J, Kucharski F, Kirk-Davidoff D, et al. Climate model shows large-scale wind and solar farms in the Sahara increase rain and vegetation. Science 2018;361:1019–22.
[67] Hasan A, Alnoman H, Rashid Y. Impact of integrated photovoltaic-phase change material system on building energy efficiency in hot climate. Energy Build 2016; 130:495–505.
[68] Heusinger J, Broadbent AM, Krayenhoff ES, Weber S. Adaptation of a photovoltaic energy balance model for rooftop applications. Build Environ 2021;192:107628.
[69] Heusinger J, Broadbent AM, Sailor DJ, Georgescu M. Introduction, evaluation and application of an energy balance model for photovoltaic modules. Sol Energy 2020; 195:382–95.
[70] Khan A, Anand P, Garshasbi S, Khatun R, Khorat S, Hamdi R, et al. Rooftop photovoltaic solar panels warm up and cool Down cities. Nature Cities 2024;1: 780–90.
[71] Chen L, Sun Y, Zhang N, Yang J, Wang D. Quantifying the benefits of BIPV windows in urban environment under climate change: a comparison of three Chinese cities. Renew Energy 2024;221:119740.
[72] Li XC, Zhao L, Qin Y, Oleson K, Zhang Y. Elevated urban energy risks due to climate-driven biophysical feedbacks. Nat Clim Change 2024:1–8.
[73] Genchi Y, Ishisaki M, Ohashi Y, Kikegawa Y, Takahashi H, Inaba A. Impacts of large-scale photovoltaic panel installation on the heat island effect in Tokyo. In: Fifth conference on the urban climate; 2003.
[74] Hirano Y, Yoshida Y. Assessing the effects of CO2 reduction strategies on heat islands in urban areas. Sustain Cities Soc 2016;26:383–92.
[75] Chen L, Zheng X, Yang J, Yoon JH. Impact of BIPV windows on building energy consumption in street canyons: model development and validation. Energy Build 2021;249:111207.
[76] Takane Y, Kikegawa Y, Nakajima K, Kusaka H. SLUCM+ BEM (v1. 0): a simple parameterisation for dynamic anthropogenic heat and electricity consumption in WRF-Urban (v4. 3.2). Geosci Model Dev (GMD) 2024;17:8639–64.
[77] Chen L, Yang J, Zheng X. Modelling the impact of building energy consumption on urban thermal environment: the bias of the inventory approach. Urban Clim 2024; 53:101802.
[78] Fthenakis V, Yu Y. Analysis of the potential for a heat island effect in large solar farms. In: 2013 IEEE 39th photovoltaic specialists conference (PVSC). IEEE; 2013. p. 3362–6.
[79] Stern R, Muller JD, Rotenberg E, Amer M, Segev L, Yakir D. Photovoltaic fields largely outperform afforestation efficiency in global climate change mitigation strategies. PNAS nexus 2023;2:pgad352.
[80] Nemet GF. Net radiative forcing from widespread deployment of photovoltaics. Environ Sci Technol 2009;43:2173–8.
[81] Zhang Z, Qian Z, Chen M, Zhu R, Zhang F, Zhong T, et al. Worldwide rooftop photovoltaic electricity generation may mitigate global warming. Nat Clim Change 2025:1–10.
[82] Mani M, Pillai R. Impact of dust on solar photovoltaic (PV) performance: research status, challenges and recommendations. Renew Sustain Energy Rev 2010;14: 3124–31.